



저작자표시-비영리-변경금지 2.0 대한민국

이용자는 아래의 조건을 따르는 경우에 한하여 자유롭게

- 이 저작물을 복제, 배포, 전송, 전시, 공연 및 방송할 수 있습니다.

다음과 같은 조건을 따라야 합니다:



저작자표시. 귀하는 원저작자를 표시하여야 합니다.



비영리. 귀하는 이 저작물을 영리 목적으로 이용할 수 없습니다.



변경금지. 귀하는 이 저작물을 개작, 변형 또는 가공할 수 없습니다.

- 귀하는, 이 저작물의 재이용이나 배포의 경우, 이 저작물에 적용된 이용허락조건을 명확하게 나타내어야 합니다.
- 저작권자로부터 별도의 허가를 받으면 이러한 조건들은 적용되지 않습니다.

저작권법에 따른 이용자의 권리는 위의 내용에 의하여 영향을 받지 않습니다.

이것은 [이용허락규약\(Legal Code\)](#)을 이해하기 쉽게 요약한 것입니다.

[Disclaimer](#)

공학박사 학위논문

**Multi-level Optimization of
Aircraft Structure
using a Physics-based Parametric
Design Framework**

매개변수 모델링이 가능한
물리 기반 설계 프레임워크를 이용한
항공기 구조물의 다중레벨 최적화

2015 년 8 월

서울대학교 대학원
기계항공공학부 우주항공공학전공
홍 단 비

Multi-level Optimization of Aircraft Structure using a Physics-based Parametric Design Framework

매개변수 모델링이 가능한
물리 기반 설계 프레임워크를 이용한
항공기 구조물의 다중레벨 최적화

지도 교수 김 승 조

이 논문을 공학박사 학위논문으로 제출함

2015 년 6 월

서울대학교 대학원

기계항공공학부 우주항공공학전공

홍 단 비

홍단비의 공학박사 학위논문을 인준함

2015 년 6 월

위 원 장 _____ (인)

부위원장 _____ (인)

위 원 _____ (인)

위 원 _____ (인)

위 원 _____ (인)

Abstract

In this study, the new design framework, DIAMOND/AIRCRAFT, is developed, which is applicable to the early design phase for aircraft. The design framework using the parametric modeling technique and automated mesh generation enables efficiently processing the labor-intensive and iterative model generation or updating whenever design changes occur. It should be also highlighted that the design framework can estimate the structural weight based on a physics-based approach using the high-fidelity method.

Multi-level optimization routine using augmented Lagrangian Method (ALM) is developed to efficiently perform the optimization for aircraft structure. It is widely known that multi-level approach is adequate to solving a large scale problem such as complex aerospace structure. By help of ALM, the highly nonlinear local constraints such as crippling, buckling and material strength can be processed with numerical stability. Various design criteria such as buckling, crippling, and material strength for beam and shell structures are taken into account. Considering a local post-buckling, Effective width method is also utilized in the structural design to achieve the goal of weight saving. The effective width is simplified as a function of skin thickness by the introduction of appropriate physical assumption to improve the computational efficiency.

As a case study, the preliminary structural sizing of wing for 90-seat turboprop aircraft is performed. With the parametric modeling function of

DIAMOND/ AIRCRAFT, elapsed time for generating FE model can be considerably reduced up to only a few minutes, while it takes several days to generate FE model of aircraft with a conventional FE modeler. Based on the more realistic model, the weight estimation from the physics-based method makes a good agreement with the reference weight more accurately. It is expected that the value of physics-based design framework will stand out when an unconventional advanced aircraft with no empirical weight data is developed rather than a conventional ‘tube-and-wing’ aircraft.

**Keywords: Multi-level Optimization, Parametric Modeling,
Physics-based Method, Design Framework,
Preliminary Structural Sizing, Weight Estimation**

Student Number: 2010-30201

Table of Contents

Chapter 1 Introduction.....	1
1.1 Background	1
1.2 Motivation	10
1.3 Research Objectives	11
1.4 Organization of Dissertation	12
Chapter 2 Development of Design Framework.....	13
2.1 Overview	13
2.2 Literature Survey	16
2.3 Heritage from ASTL	18
2.4 Design Framework using Parametric Modeling	20
2.4.1 <i>Wing Generator</i>	20
2.4.2 <i>Fuselage Generator</i>	25
2.4.3 <i>Empennage Generator</i>	30
Chapter 3 Design Criteria	34
3.1 Overview	34
3.2 Buckling Criteria	35
3.2.1 <i>Column Buckling</i>	35
3.2.2 <i>Shell Buckling</i>	38
3.3 Crippling Criteria	43
3.4 Johnson-Euler Interaction Equation	50
3.5 Material Strength	52
Chapter 4 Multi-level Optimization	53
4.1 Overview	53

4.2 Literature Survey	54
4.3 Global Level vs. Local Level in MLO	59
4.4 Augmented Lagrangian Method	61
4.4.1 <i>Mathematical Formulation</i>	61
4.4.2 <i>Test Problem for Code Validation</i>	67
4.5 Calculation of Gradient and Hessian Matrix	71
4.5.1 <i>Gradient of Constraint Functions for Beam</i>	71
4.5.2 <i>Hessian of Constraint Functions for Beam</i>	74
4.5.3 <i>Gradient of Constraint Functions for Shell</i>	75
4.5.4 <i>Hessian of Constraint Functions for Shell</i>	78
Chapter 5 Preliminary Structural Sizing.....	79
5.1 Overview	79
5.2 General Information	80
5.2.1 <i>Aircraft Configuration</i>	80
5.2.2 <i>Material Selection</i>	80
5.3 Problem Statement	84
5.4 Effective Width Method	86
5.5 Computational Results	89
5.5.1 <i>Load Generation</i>	89
5.5.2 <i>Minimum Weight Design</i>	93
5.5.3 <i>Parametric Study</i>	97
5.5.4 <i>Comparison with Empirical Methods</i>	101
Chapter 6 Conclusion	103
Bibliography	105
Appendix	111

List of Figures

Figure 1.1	Schematic Outline of Design Process in the Early Design Phase	6
Figure 1.2	Iterative Development Method in Concurrent Engineering.....	8
Figure 1.3	Status of Various Design Features during the Design Process	9
Figure 2.1	Composition of DIAMOND/AIRCRAFT	14
Figure 2.2	Design Procedure in DIAMOND/AIRCRAFT	15
Figure 2.3	Feature of DIAMOND/IPSAP	19
Figure 2.4	Airfoil Information for Main Wing.....	22
Figure 2.5	GUI for Wing Parameters	22
Figure 2.6	FE Model of Wing via Parametric Modeling.....	24
Figure 2.7	GUI for Center Fuselage Parameters	27
Figure 2.8	GUI for Aft Center Fuselage Parameters	27
Figure 2.9	GUI for Aft Fuselage Parameters.....	28
Figure 2.10	FE Model of Fuselage via Parametric Modeling	28
Figure 2.11	GUI for Empennage Parameters: Vertical Tail.....	30
Figure 2.12	GUI for Empennage Parameters: Horizontal Tail	31
Figure 2.13	FE Model of Empennage via Parametric Modeling.....	31
Figure 2.14	FE Model of Entire Aircraft via Parametric Modeling	33
Figure 3.1	Column End Fixity Coefficients	37
Figure 3.2	Compressive Buckling Coefficients for Flat Rectangular Plates	40
Figure 3.3	Shear Buckling Coefficients for Flat Rectangular Plates.....	41
Figure 3.4	Interaction Equation for Combined Shear and Compression	42

Figure 3.5	Cross Section Subjected to Crippling Stress.....	43
Figure 3.6	Dimensionless Crippling Stress vs. b'/t	46
Figure 3.7	Johnson-Euler Interaction Curve	51
Figure 4.1	Flow Chart for Multi-level Optimization.....	58
Figure 4.2	Global Level and Local Level in MLO.....	60
Figure 4.3	Flowchart of Augmented Lagrangian Method (ALM)	65
Figure 4.4	Flowchart of Newton Method in ALM	66
Figure 4.5	Convergence History of Design Variables	69
Figure 4.6	Convergence History of Objective Function	69
Figure 5.1	Configuration of 90-seat Turboprop Aircraft.....	81
Figure 5.2	Plan View of Wing Layout (Half Span)	82
Figure 5.3	Stress Distribution before and after Buckling.....	88
Figure 5.4	Data Transfer Technique between Dissimilar Meshes	91
Figure 5.5	V-M-T Curves for Applied Load Condition.....	92
Figure 5.6	Convergence History of Wing Weight	95
Figure 5.7	Distribution of Upper Skin Thickness	96
Figure 5.8	Distribution of Lower Skin Thickness	96
Figure 5.9	Wing Weight vs. the Number of Stringers	99
Figure 5.10	Wing Weight Breakdown for the Number of Stringers.....	99
Figure 5.11	Wing Weight vs. the Number of Ribs	100
Figure 5.12	Wing Weight Breakdown for the Number of Ribs.....	100
Figure 5.13	GUI of COCOA for Empirical Weight Estimation	102

List of Tables

Table 1.1	Summary of Design Phases	7
Table 2.1	Design Parameters for Wing	23
Table 2.2	Design Parameters for Fuselage	29
Table 2.3	Design Parameters for Empennage	32
Table 3.1	Basic Angle Unit for Edge Conditions	47
Table 3.2	g values for Various Cross Sections in Gerard Method	48
Table 3.3	Maximum Values for Crippling Stress	49
Table 4.1	History of Constraint Functions	70
Table 5.1	Geometry Information of Wing	83
Table 5.2	Material Selection for Wing Component	83
Table 5.3	Comparison of Weight Estimations for Wing	102

Chapter 1 Introduction

1.1 Background

The design process of an aircraft is generally broken down into three following phases: conceptual design, preliminary design, and detail design. Such a series of design process is full of various decision-makings for the reliable and affordable design, which can successfully satisfy requirements of the product with respect to both performance and cost. As shown in Figure 1.1, conceptual design starts from design requirements. Such design requirements is generally known as Top Level Requirements (TLRs), which will represent the direction of the aircraft design. In order to find the feasible aircraft design satisfying all design requirements considered, a myriad of design candidates should be reviewed and modified again and again through the exploration of design space.

The objective of conceptual design phase is to investigate and compare various design candidates in order to determine a feasible layout of aircraft which is technically excellent and economically competent, a baseline configuration. In this design phase, preliminary aircraft performance is also predicted, and the size and placement of the major vehicle components is assigned. For example, primary components such as wing, fuselage, nacelles, empennage and other systems are provisionally sized to be reflected onto a baseline configuration. Once determining a baseline configuration, aircraft design engineers will enter next preliminary design phase. Preliminary design is characterized as setting goals for the design tasks to be performed in the

next detail design phase. Table 1.1 represents the summary of three design phases aforementioned.

Design process is inevitably iterative by nature and concurrently interactive between multi-disciplines, even in a single discipline. During the design process, a number of disciplines should persistently communicate with each other, while each discipline has autonomy. This is the reason why concurrent engineering has been adapted for use especially in the aerospace industry. In concurrent engineering[1,2], an integrated and iterative development method, as shown in Figure 1.2, is adopted to enhance product development efficiency. This kind of method is so eligible for the aircraft development that most of all, an efficient design tool is indispensable for the effective implementation of concurrent engineering.[3] During the early phase of design process for performing trade-off studies, design engineers should construct and modify geometric models manually and frequently using three-dimensional Computer-Aided Design (CAD) software whenever design changes occur. Then the geometry based on CAD model is generally converted to meta-models for analysis. From the viewpoint of structure discipline, Finite Element (FE) model generation task is still very tedious and time-consuming. Therefore, the automated design framework using parametric modeling[4–14] can alleviate more remarkably the burden of such an iterative and labor-intensive process.

Figure 1.3 shows the status of various design features during the design process. It means that there will be a large portion of commitment in terms of configuration, manufacturing technology, and maintenance

techniques at the early phase of development program. During conceptual or preliminary design phase, the maturity of design is inevitably low and limited because the information on the definition of an aircraft may be unavailable partly or be not detailed in general. Because of the same reason, until now, low fidelity methods have been generally preferred to high fidelity ones for simple and fast iteration cycles because available resources such as computational time and cost are also limited considerably in the early design phase. Nowadays, this problem occurred by limited resources can be overcome with a relatively cheaper computer with high computational capability than in the past. Recently, the attempt to introduce high fidelity method earlier has been attracting attention with keen interest with the help of such high performance computing capability. Especially, the design of advanced or unconventional aircraft requires that high-fidelity and physics-based method be used earlier.[15] The availability of high fidelity method in the early design phase has strong relation with the cost reduction.

It is definitely remarkable that decisions made in this early phase have an enormous and far-reaching influence on the later design phases with respect to cost as well as performance. Enterprise-based life cycles consist of five distinct functional phases: (1) assessment of opportunities, (2) investment decision, (3) system concept development, (4) subsystem design and pre-deployment, and (5) deployment/installation, operations, support, and disposal.[16] According to Rizzi[17], the importance of early design phases is worthy of notice in that 80% of the life cycle cost of an aircraft is determined by decisions taken during the early design phase. As the design process

progresses, product-specific knowledge is gradually accumulated, but change in design is getting harder and harder as shown in Figure 1.3. It means that even a small design change may incur more additional cost than it did. Hence, it is essential to ensure the high confidence and the low risk in decisions made at the early phase with the help of high fidelity methods. Consequently, the use of high fidelity methods such as Finite Element Method (FEM) and Computational Fluid Dynamics (CFD) enables reducing development risk resulted from the growth of structural weight.

Aerospace structures should bear all possible design loads expected and be also designed with optimal structural weight satisfying a variety of requirements. Hence, from the early design phase, the main interest of design engineers is to accurately estimate and control the structural weight, preferably with a high degree of fidelity.[9,18–20] The primary objective of physics-based design framework is to improve a level of prediction accuracy for the weight of structure with load-carrying capacity as highly as possible. So far, various methods of weight estimation have been used for aircraft design, which are categorized into different classes.

Most of methods generally have started from empirical approach based on statistical database for similar aircrafts in size.[21–24] These methods are generally called low class methods including Class I and II methods. The Class I method estimates weight of major aircraft components as a percentage of Maximum Take-Off Weight (MTOW). The averaged figure of actual weight data from a number of existing aircrafts is calculated as the first guessing of the weight for each component. Class II method is introduced

to predict the weight of major components, in more detail than class I method, from semi-empirical equation or statistical data when the baseline configuration of an aircraft is determined. Since Shanley[25], class II & 1/2 methods have been also proposed, which are quasi-analytic methods that utilize elementary stiffness/strength analysis of structures.[26] PDCYL implemented by NASA is one of the software for class II & 1/2 method.

Class III method is categorized into a physics-based approach based on the high fidelity method such as FEM. This kind of method calculates the structural weight using physical measurement such as volume and material density, not from statistical data. Although class III method is superior to lower class methods including class I and class II methods with respect to accuracy, it requires much more specific information in detail than lower ones. When the required information may be partly unavailable in the early design phase, such a problem due to the absent data can be overcome through the mixed use of data from empirical data.

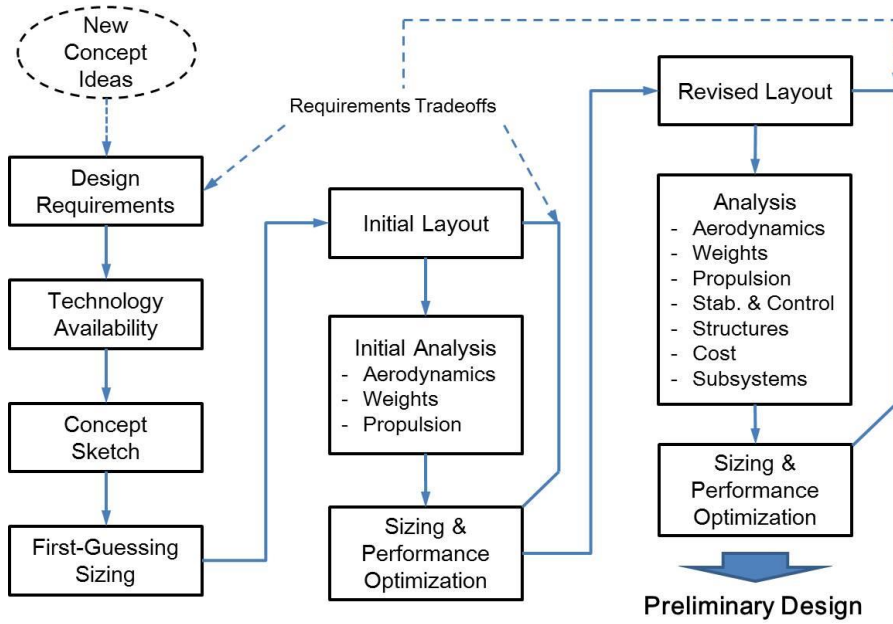


Figure 1.1 Schematic Outline of Design Process in the Early Design Phase [27]

Table 1.1 Summary of Design Phases [16]

Phase	Conceptual Design	Preliminary Design	Detail Design
Phase Gate	Conceptual Design Review	Preliminary Design Review	Critical Design Review
Design Product	- Functional baseline - Design-to package	- Allocated baseline	- Product baseline - Build-to package
Design Activities	- Requirement analysis - Evaluation of feasible technology - Selection of technical approach	- Requirements allocation - Trade-off study - Synthesis - Preliminary design	- Subsystem design - Development of engineering models - Verification of manufacturing and production processes

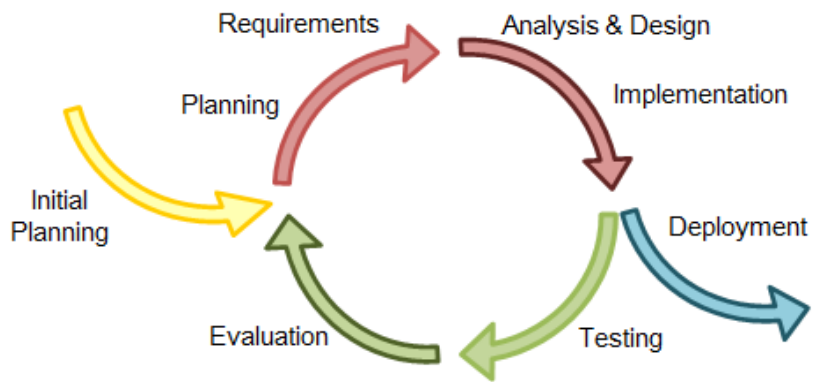


Figure 1.2 Iterative Development Method in Concurrent Engineering [28]

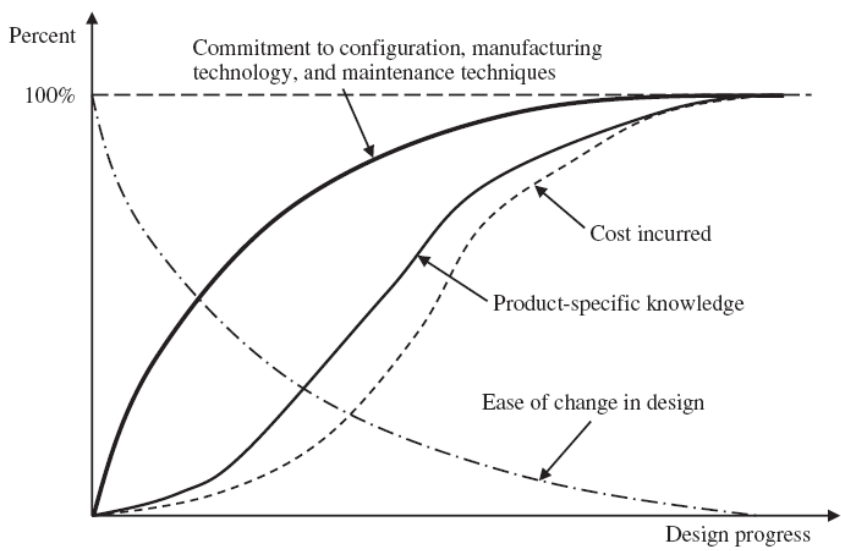


Figure 1.3 Status of Various Design Features during the Design Process [2]

1.2 Motivation

From the start of conceptual design, the geometry generation usually relies on CAD software. Actually, most of the aircraft manufacturers have selected CAD software as a geometry modeler. Generally, CAD has its own strengths to improve the productivity of design engineer, the quality of design, and communications between design engineers through hierarchical documentation of design change. The core features of CAD also involve high precision, flexibility, and especially the relation with manufacturing. Unfortunately, such features are more appropriate for the phase after preliminary design than for early design phases. Furthermore, the crucial problem is that the way of defining geometry in CAD is basically different from how engineers define the geometry of an aircraft.[6] Although CAD software can build a detailed geometric model, a considerable amount of time and efforts for becoming proficient is demanded. Accordingly, CAD-based modeling may be detrimental to efficiency and become hindrances during the early design phase. It is highly recommended to utilize parameters defining the aircraft configuration such as span, chord lengths, sweepback angle, and the like in order to generate the aircraft geometry.[5]

1.3 Research Objectives

This dissertation deals with the following objectives for the development of the aircraft design framework and its optimization routine.

Objective 1: Develop a physics-based design framework using parametric modeling.

The term physics-based means that the design framework is not dependent on empirical data for existing aircrafts. The parametric modeling technique should be used to enable efficient design space exploration during the early design phase.

Objective 2: Implement the multi-level optimization routine using Augmented Lagrangian Method (ALM).

Multi-level optimization algorithm is implemented to solve a large-scale problem easily by decomposing it into a set of small problem, where ALM is utilized to handle constraint functions efficiently using multipliers terms.

Objective 3: Apply various design criteria such as buckling, crippling, local post-buckling, and the like to the optimization process.

Various design criteria play roles of constraints during the optimization process. The more design criteria we consider, the more reliable structure close to real we can design. Using effective width method, a local post-buckling analysis is also taken into account for lighter structure.

1.4 Organization of Dissertation

The dissertation consists of totally 6 chapters, including this chapter, and Appendix.

Chapter 2 describes the development of aircraft design framework for preliminary design phase. The design framework uses the parametric modeling technique to make the design process more efficient and productive.

Chapter 3 deals with various design criteria for structural sizing. The design criteria include buckling for both beam and shell, crippling for beam, material strength. Additionally, Johnson-Euler interaction equation is also considered for the evaluation of structural integrity.

Chapter 4 describes Multi-level Optimization (MLO) algorithm using augmented Lagrangian method (ALM). The concept of MLO is briefly outlined, and the formulation of ALM is arranged in the following part. The various design criteria mentioned in Chapter 3 are taken into account constraint functions for optimization process.

Chapter 5 represents physics-based design optimization. The wing design of 90-seater regional aircraft is performed. Results using multi-level optimization with respect to various design variables are shown. The weight calculated by physics-based method is compared with those from empirical methods.

In Chapter 6 as the final chapter, the achievements and contributions of this dissertation are summarized.

Chapter 2 Development of Design Framework

2.1 Overview

So far, enormous efforts have been made to construct the integrated design tool for Multi-disciplinary Design Optimization (MDO) in order to solve complex and involved design problems efficiently because the aircraft design is very interactive activity incorporating a number of disciplines such as aerodynamics, structure, control, and so on.[29] The scope of the chapter is presently focused on the design framework only for structural design during conceptual and preliminary design phase.

Our design framework is designated as ‘DIAMOND/AIRCRAFT’. Figure 2.1 shows composition of the design framework, which has three generators for OML and FE model generation as follows: wing generator, fuselage generator, and empennage generator. First, the outer mold line (OML) of aircraft is defined through those generators using parametric modeling technique. The internal structural layout is also determined at the same time, which is followed by FE mesh generation. With the design loads applied to FE mesh, structural members are sized through a physics-based approach, FEM. At this moment, various design criteria are considered as constraints of optimization, and multi-level optimization method is adopted to enhance computational efficiency for faster convergence. The application of a high fidelity method such as FEM is desirable in order to increase the confidence for decision-making and reduce the design risk. Figure 2.2 shows the design procedure for aircraft design using DIAMOND/AIRCRAFT.

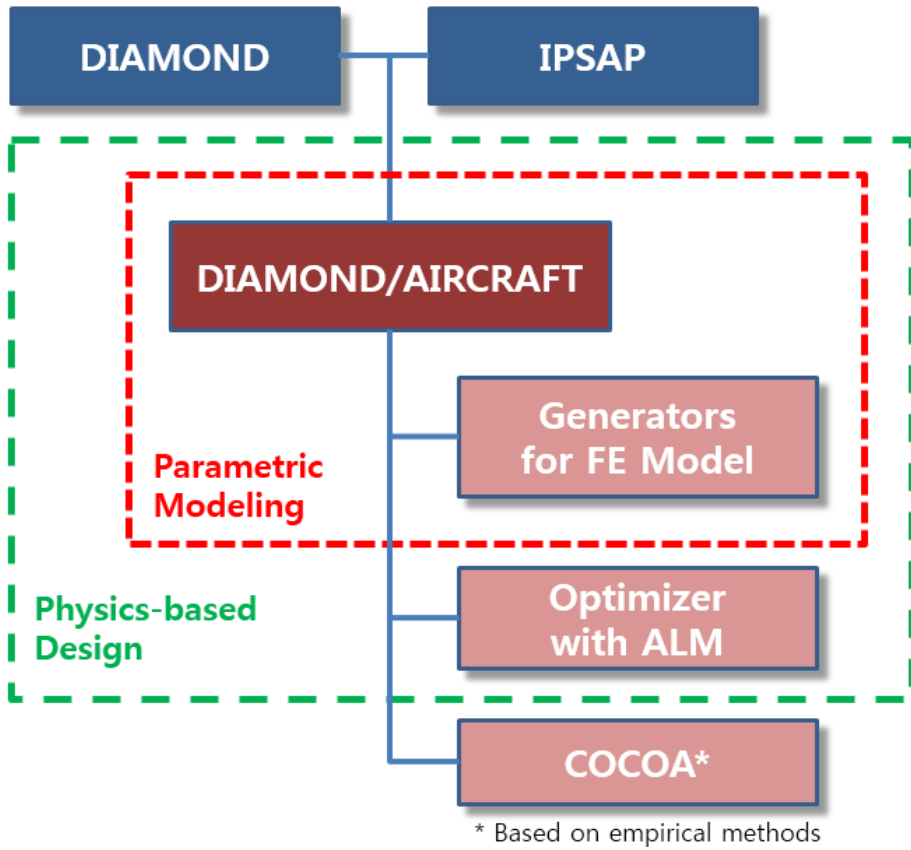


Figure 2.1 Composition of DIAMOND/AIRCRAFT

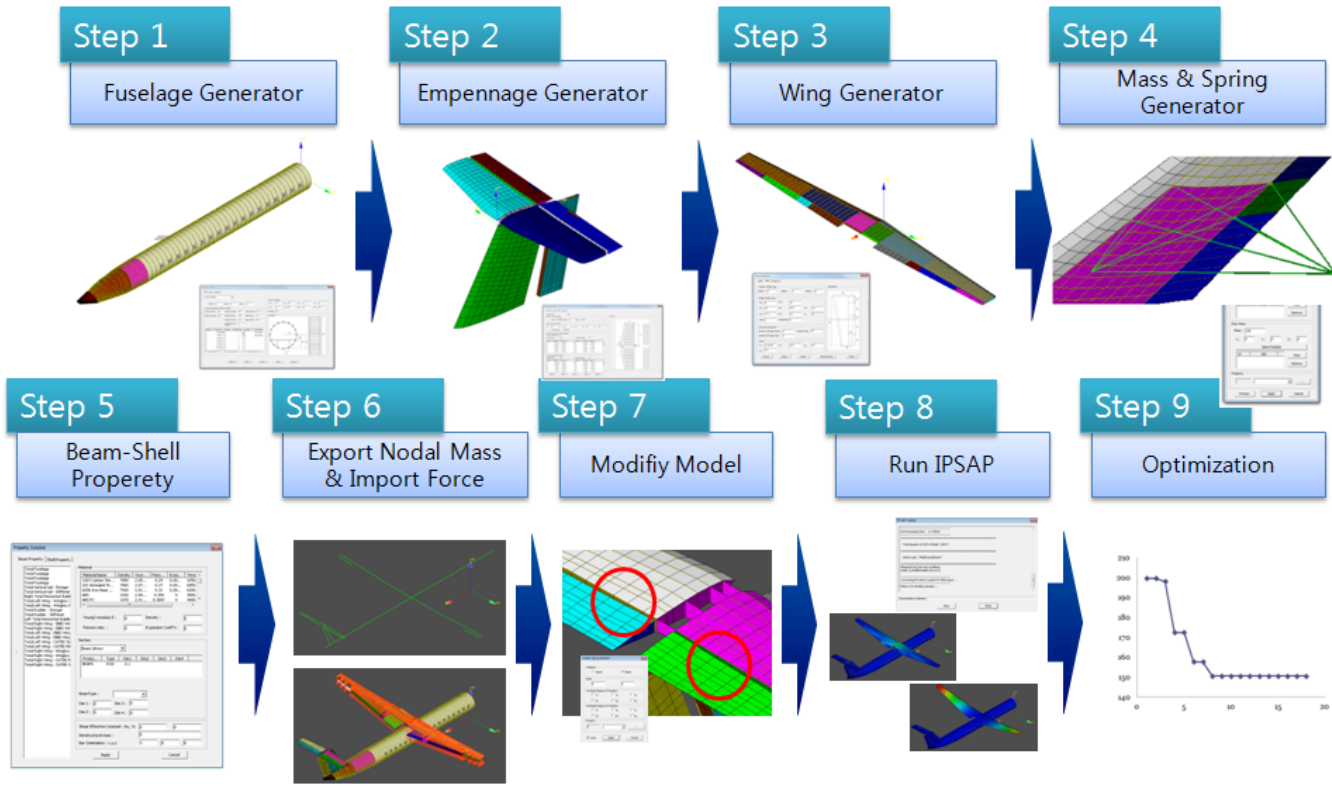


Figure 2.2 Design Procedure in DIAMOND/AIRCRAFT

2.2 Literature Survey

The necessity of parametric modeling for aircraft design is evidently recognized in Chapter 1. Now, the previous studies for parametric modeling by other researchers are investigated to understand their contents of research.

Mawhinney et al. [7] proposed geometry-based approach for aircraft conceptual design to efficiently integrate the analysis and design method. They show that aircraft geometry is generated with the use of displacement, rotation, and profile components. Using the geometric information, three kinds of geometric models can be generated for the related analysis: skeleton, and surface, and solid models. The skeleton model is suitable for loading and structural analysis, while the surface and solid models are for aerodynamic analysis. Consequently, the model for structural analysis is unrealistic and undesirable in terms of the level of fidelity. Rodriguez et al. [5] developed RAGE (RAPid Geometry Engine) in order to create the aircraft geometry for preliminary design analysis without excessively sophisticated CAD. RAGE is composed in object-oriented JAVA programming language. RAGE utilizes a component-based approach to generate geometric models of the aircraft. Main components include fuselages, wings, and nacelles. They claimed that the geometric model is mathematically built using the design parameters directly in RAGE unlike in CAD software that creates splined surfaces. RAGE can export geometric models formats for aerodynamic analysis tools such as PLOT3D and PANAIR. La Rocca et al. [30] proposed high-level geometry primitives in order to help the design engineer generate automated aircraft geometry. Once picking parameterized geometric elements from database

instead of CAD-based elements such as points, lines, and curves, the design engineer can obtain the geometry of a concept configuration. Although the proposed method makes the design process efficient and productive through fast performance, the fidelity is limited and difficult to expand due to the code-based characteristics.

Researchers working at NASA proposed RAM (Rapid Airplane Modeler) [4] and VSP (Vehicle Sketch Pad) [6], sequentially released in 1996 and 2010, respectively. RAM was developed written in C++ language to generate 3-D geometry of aircraft quickly and easily in user-friendly environment for conceptual design. There are four main components in RAM: wing, fuselage, external store such as fuel tank and missiles, and engine including nacelle and duct. Each component is defined by its own parameters. But, it shows a limited capability to export the geometric model in formats for vortex lattice method (VLM) and CFD analysis. With the successful experience of developing RAM, VSP was developed as a modified and advanced modeler. It enables improving the ability to easily define geometry by design parameters and displaying in real-time the results of such geometric definition on GUI. VSP was simply used to provide synthesis code such as ACSYNT and FLOPS with wetted areas and volumes of an aircraft. VSP can also generate meta-models to perform high fidelity method, for example, AWAVE (supersonic compressibility drag analysis program), VorLax (vortex lattice flow solver), FPS3D (full potential flow solver), and MUSEC (Euler flow solver). Similar to RAGE and RAM, however, VSP concentrates on the meta-model generation mostly for aerodynamic analysis as well. For

structural analysis, VSP is capable of generating only elements with full depth such as ribs, spars, and bulkheads for internal structural layout, while it cannot generate partial depth elements such as stringers and stiffeners for the detailed modeling of structure.

2.3 Heritage from ASTL

The main objective of DIAMOND/AIRCRAFT is to improve the design process efficiency and accuracy through a parametric modeling and physics-based approach using finite element analysis. In order to design structural components close to real ones as accurately as possible, various design criteria can be selectively applied to structural sizing. Most of functions of DIAMOND/AIRCRAFT are implemented under the environment of DIAMOND/IPSAP, which is the integrated finite element analysis software with OpenCASCADE-based Graphic User Interface (GUI) for pre/post processing. DIAMOND/IPSAP was developed and released by ASTL (Aerospace Structures Laboratory) of the Seoul National University. This software enables parallel computing process using domain-wise MFS (Multi Frontal Solver) as well as serial computing process, thus showing excellent performance speed and improved computational accuracy for finite element analysis. Hence, DIAMOND/IPSAP has the advantage of computational capability adequate to solve large-scale problems for complex aerospace structures such as aircraft, satellite, and launch vehicle.[31,32] It is notable that DIAMOND/AIRCRAFT has accordingly such an excellent heritage from DIAMOND/IPSAP.

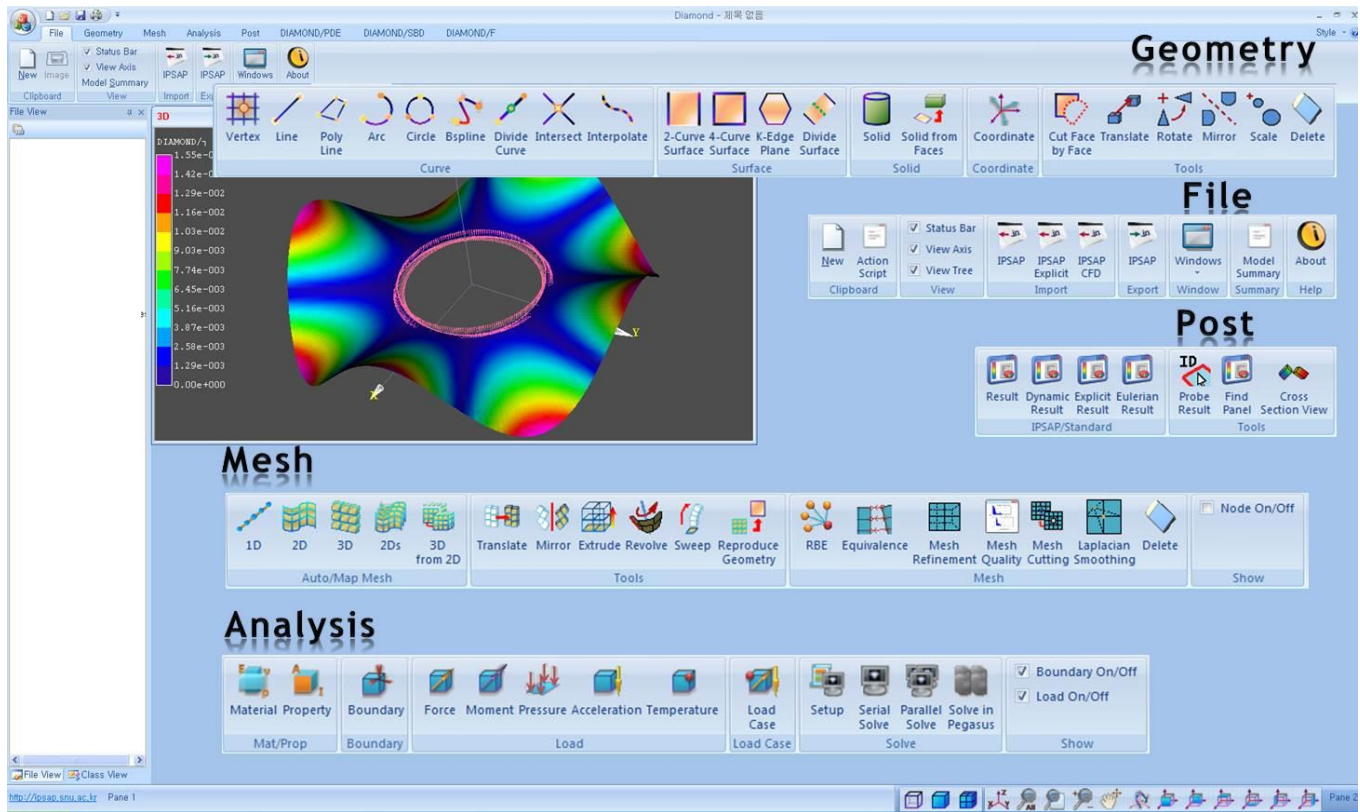


Figure 2.3 Feature of DIAMOND/IPSAP

2.4 Design Framework using Parametric Modeling

Each generator defines the configuration of object via handling simple parameters input and at the same time generate FE mesh for the corresponding part out of entire aircraft after reflecting internal structural layout. All results from three generators can be merged collectively when FE mesh of entire aircraft is required. The preview function of GUI is very helpful during iterative modification because the change of FE meshes can be immediately displayed and checked as soon as design parameters change.

2.4.1 Wing Generator

First of all, airfoil selection should be performed as shown Figure 2.4 in order to determine the configuration of main wing. The information on geometry of three airfoils and each location along the span-wise direction of wing are required at GUI of wing generator. Airfoil coordinates data can be imported by text file format or by manual key-in and might be amended directly on GUI if necessary

Main wing can be divided into two segments such as inboard wing and outboard wing. Wing OML can be roughly determined by chord lengths at root and tip of wing, semi-span, sweep back angle, airfoil data, and something about flaps. DIAMOND/AIRCRAFT can produce the structural model considering the secondary structure as well as the primary structure, while other similar design tools can deal with the primary structure only. For more detailed structural layout such as the chord-wise location of front and rear spars, the number of ribs, the number of stringers, and the attachment between

wingbox and secondary structures, tens of figures are needed as shown in Figure 2.5. In case of two spar structure, the front spar is typically located in the region near about 15 percent of the chord, and the rear spar at 55-60 percent. [33] The location of spars can be determined when sufficient space for the housing of control surfaces, high lift devices, their actuating systems, and de-icing device is obtainable. The locations of ribs are very important from view of structural stability because they not only postpone local buckling on the skin but also have relation to attachment of powerplants, stores, and landing gear structure. All the design parameters on GUI can be exported for the next trial or another use in the format of text file. The design parameters for wing configuration and structural layout are summarized in Table 2.1.

The center wingbox in inboard wing area withstands applied loads from flight conditions. It is widely known that the stiffened panel concept is efficient for the load-carrying structure with respect to the weight reduction, which consists of skins and stringers. In order to create FE mesh of wing, four-node shell element is utilized for modeling the upper and lower skins, the spars, the ribs, and the like, and two-node beam element for modeling the stringers, spar cap, and the like. Figure 2.6 shows FE model generated for wing via parametric modeling.

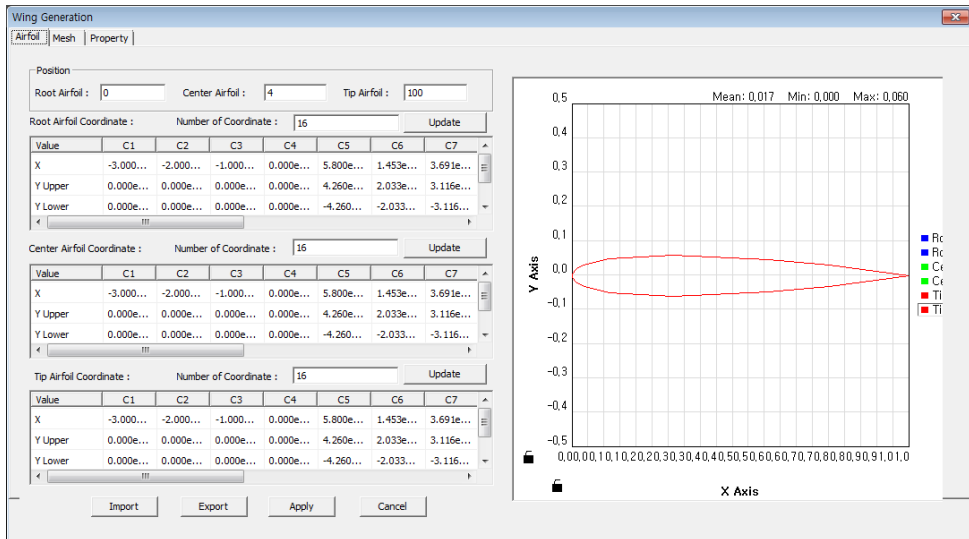


Figure 2.4 Airfoil Information for Main Wing

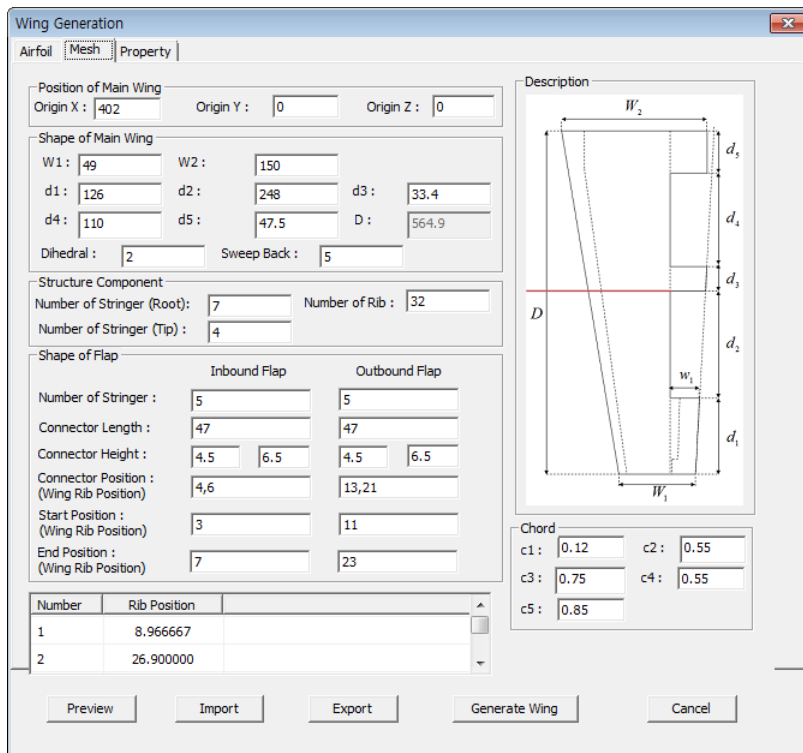


Figure 2.5 GUI for Wing Parameters

Table 2.1 Design Parameters for Wing

Purpose	Design Parameters
Configuration	Chord length at Wing Root & Tip Wing Semi-Span Sweepback Angle Dihedral Angel Location of the Flap Housing Span of Inner & Outer Flap
Structural Layout	Number of Stringers at Wing Root & Tip Number of Ribs Location of Front & Rear Spars for Wing Location of Front & Rear Spars for Inner & Outer flaps

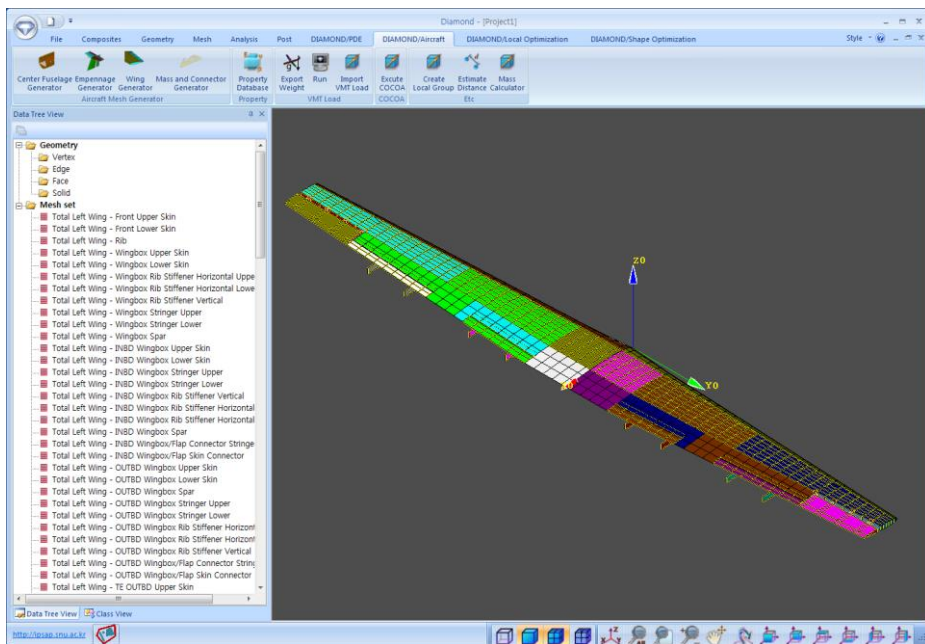


Figure 2.6 FE Model of Wing via Parametric Modeling

2.4.2 Fuselage Generator

Just as airfoil determination is the first step for wing modeling mentioned earlier, so cross section definition is for fuselage modeling. Figures 2.7-2.9 show GUIs of fuselage generator, precisely speaking, divided into center fuselage, aft center fuselage, and aft fuselage. For center fuselage with constant section, two radii are required for the definition of cross section. The data on window and door such as quantities and dimensions is required for fuselage configuration as shown in Figure 2.7. In order to define structural layout of the fuselage, the number of frames and stringers, and the location of floor and its supporting structures are needed. By default, all the frames are equally spaced along the length of center fuselage, but the location of each frame is promptly editable on GUI. Similarly, the location of stringers is equally spaced but also editable along the perimeter of fuselage. For aft fuselage, most of all, the arrangement of frames should be located after considering the attachment to empennage because there is a load path between fuselage and empennage. Some frames in aft fuselage are installed with a tilting angle in order to ensure load path from vertical stabilizer to fuselage. The design parameters for fuselage are summarized in Table 2.2.

Compared with that of wing structure, the load level of fuselage generally tends to be lower. But, when structural design is performed, special attention should be paid because fuselage structure has a number of cut-outs such as doors, windows, landing gear, and the like, which are structurally vulnerable at the outer end. Moreover, pressurization might be considered one

of load conditions, especially for skin design, because the cabin of transport aircraft is mostly pressurized. The pressurization of the cabin will be importantly allowed for from the fatigue aspect after the early design phase. In DIAMOND/AIRCRAFT, it is easy to apply the load due to pressurization to FE model of fuselage as shown in Figure 2.10.

Generally, the fuselage skin bears shear load as well as the load due to pressurization and is supported by stringers and frames to prevent stress concentration and local buckling. In DIAMOND/AIRCRAFT, fuselage skins and floor panel are modeled using four-node shell element for FE model. Fuselage skin is reinforced by frames, stringers and supporting structure, where they are modeled using two-node beam element. Figure 2.10 shows FE model of fuselage with an interface for pressurization load.

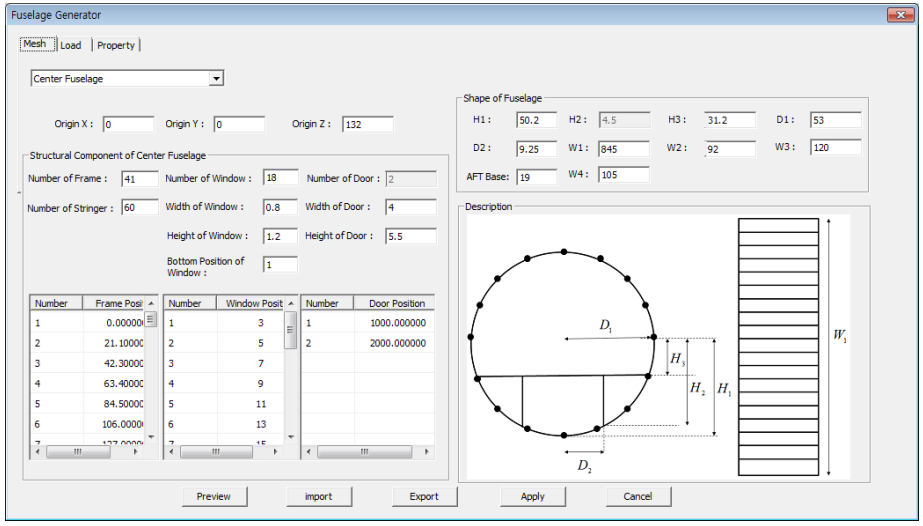


Figure 2.7 GUI for Center Fuselage Parameters

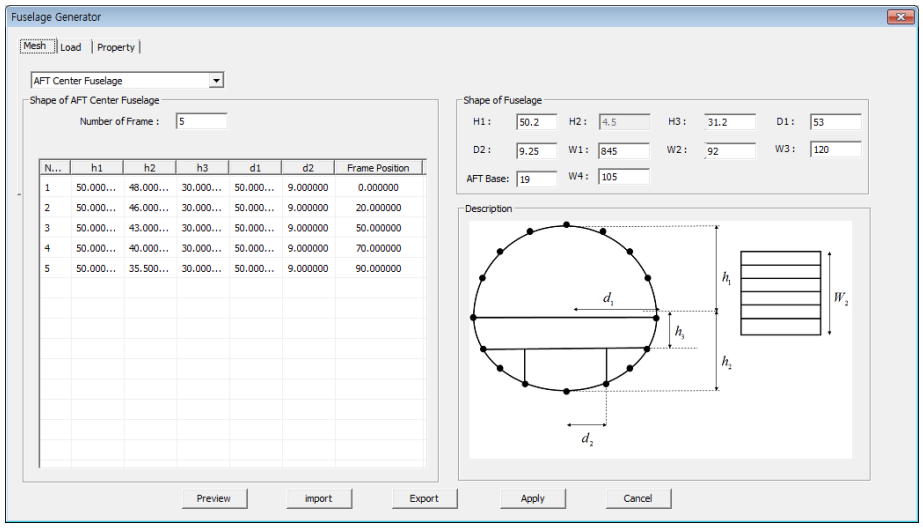


Figure 2.8 GUI for Aft Center Fuselage Parameters

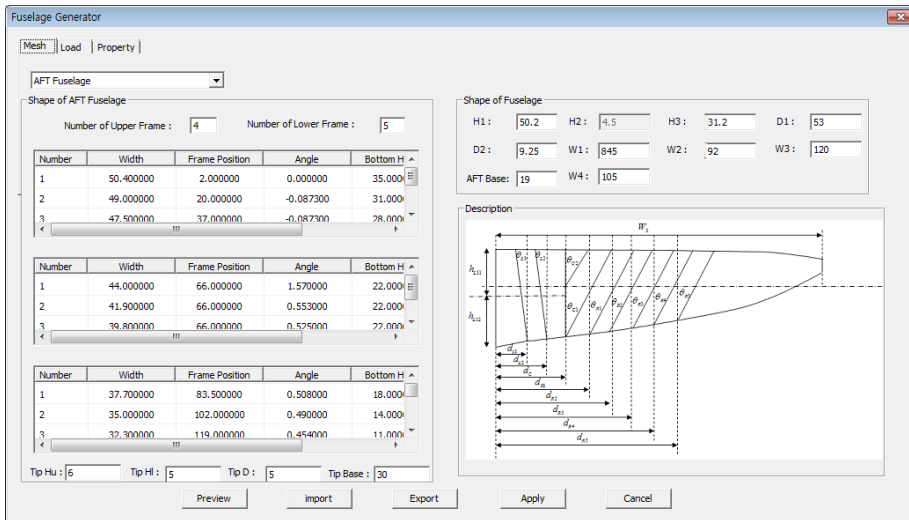


Figure 2.9 GUI for Aft Fuselage Parameters

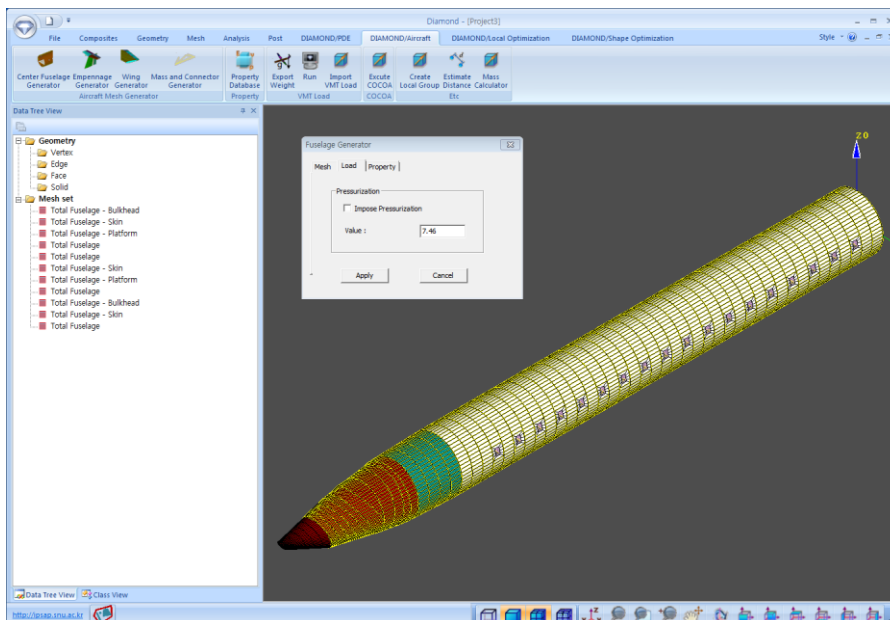


Figure 2.10 FE Model of Fuselage via Parametric Modeling

Table 2.2 Design Parameters for Fuselage

Purpose	Design Parameters	
Configuration	Center	Fuselage length Radius of Width, Radius of Height Number, Location, and Dimension of Windows Number & Dimension of Doors
	Aft Center	Fuselage length Radius of Width, Radius of Height
	Aft	Fuselage length Upper Radius, Lower Radius
Structural Layout	Center	Number of Frames Number of Stringers Location of Floor Panel Location of Supporting Structure
	Aft Center	Number of Frames Location of Floor Panel Location of Supporting Structure
	Aft	Locations and Tilt Angles of Frames

2.4.3 Empennage Generator

Most of design parameters of empennage consisting of vertical and horizontal stabilizers are basically similar to those of wing. In the same manner, each OML is defined by three airfoil coordinates, chord lengths at root and tip, and span for both of vertical and horizontal stabilizer. With respect to structural layout, empennage might be modeled as multi-cell structure with multiple spars in order to resist external loads effectively. Figures 2.11-2.12 show the GUI for parameters of vertical and horizontal tails. The design parameters for empennage configuration and structural layout are summarized in Table 2.3. Figure 2.13 shows FE model of empennage via parametric modeling. Consequently, finite element model of entire aircraft is shown in Figure 2.14 including fuselage, wing, and empennage.

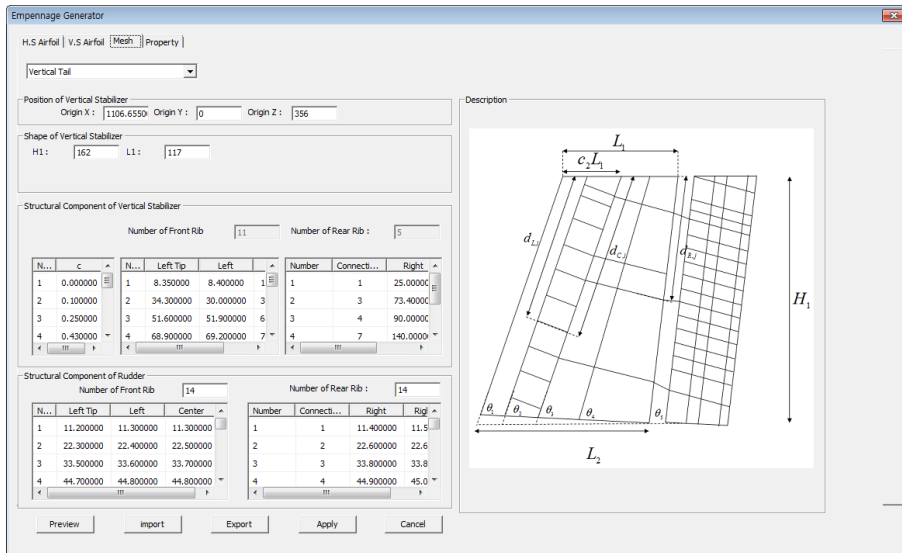


Figure 2.11 GUI for Empennage Parameters: Vertical Tail

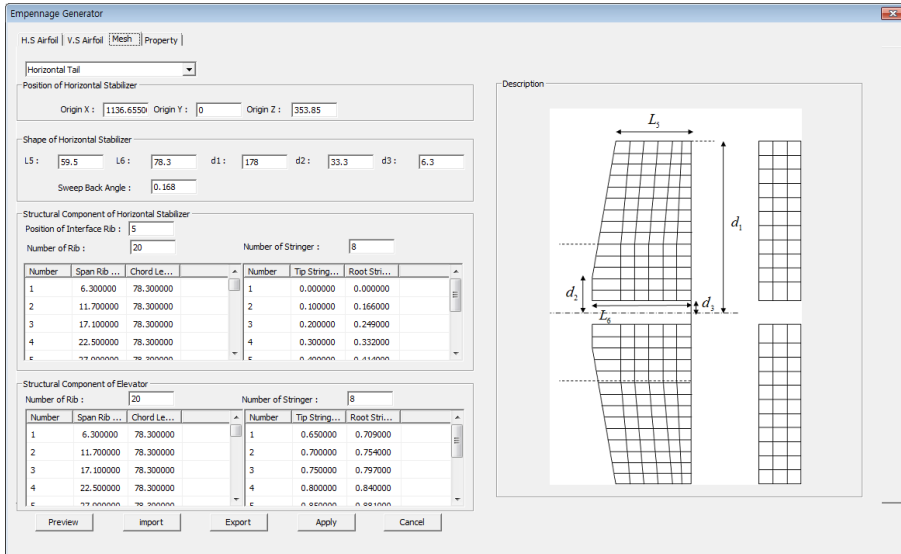


Figure 2.12 GUI for Empennage Parameters: Horizontal Tail

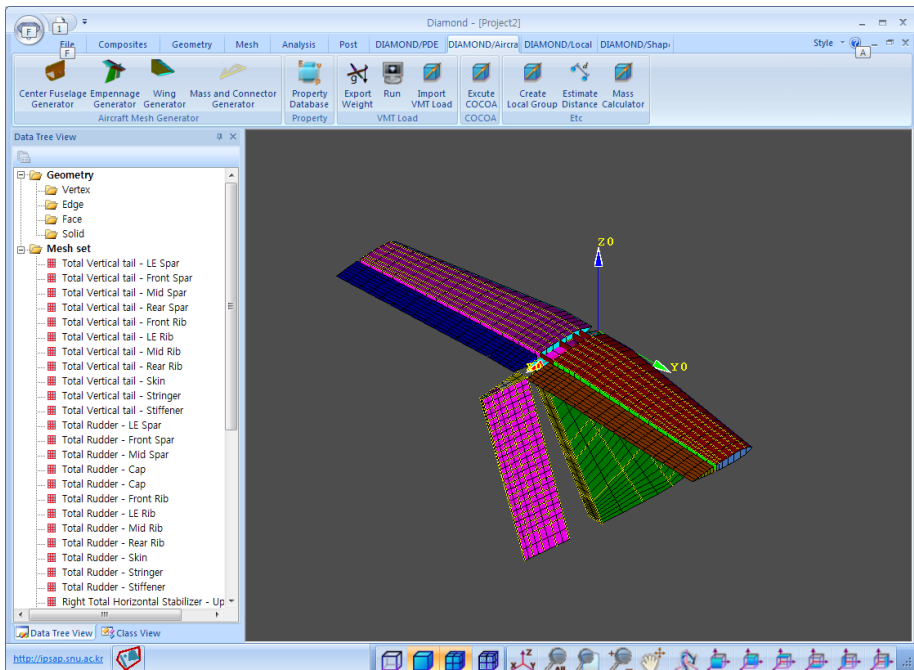


Figure 2.13 FE Model of Empennage via Parametric Modeling

Table 2.3 Design Parameters for Empennage

Purpose	Design Parameters	
Configuration	HT	Chord length at Root & Tip Semi-Span Sweepback Angle
	VT	Chord length at Root & Tip Semi-Span
Structural Layout	HT	Number of Stringers Number of Ribs Location of Interface Rib with VT Gap from the Center Line
	VT	Number of Stringers Number of Front Ribs & Rear Ribs Location and Sweepback Angle of Spars

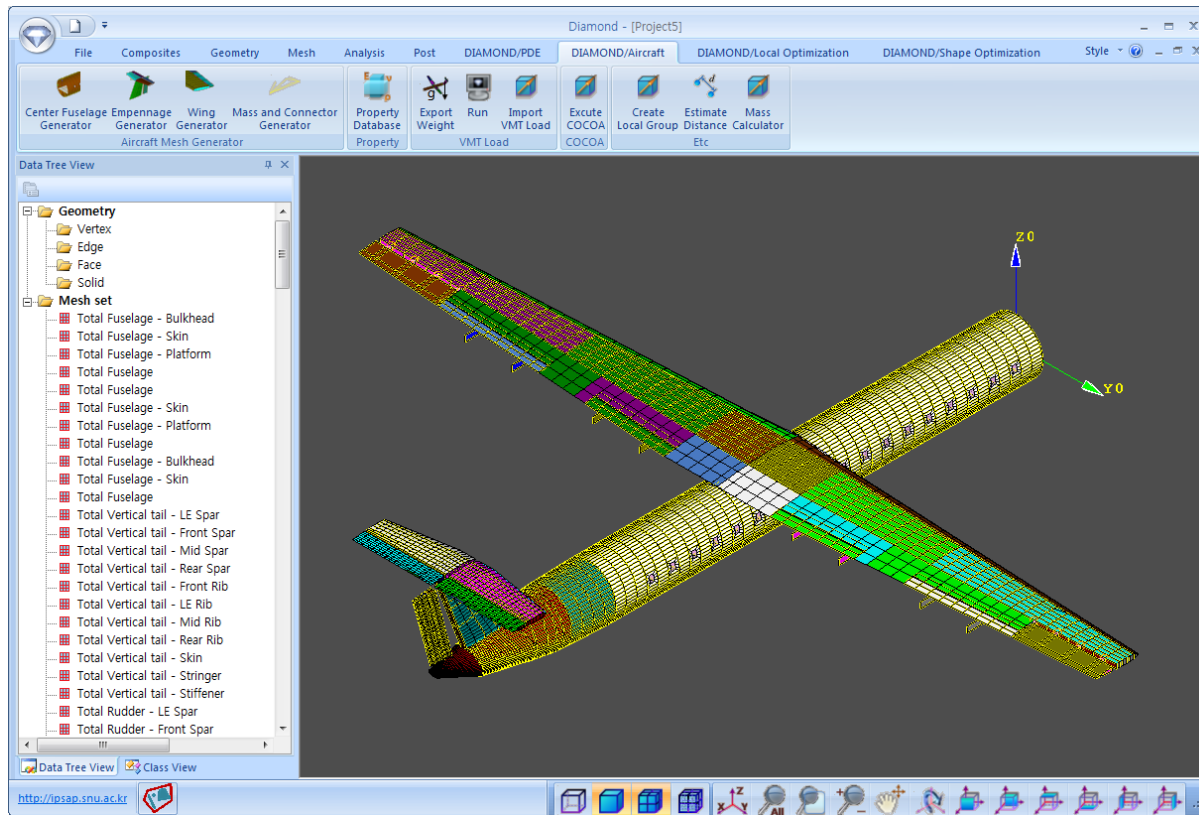


Figure 2.14 FE Model of Entire Aircraft via Parametric Modeling

Chapter 3 Design Criteria

3.1 Overview

In Chapter 2, the procedure of generating the FE structural model using parametric modeling technique is explained for a physics-based design. When FE analysis is performed with the FE model generated, design criteria must be required to evaluate whether the structure can withstand the external forces which are expected to be imposed under the design load conditions.

The conventional approaches for minimum weight design of complex aircraft structures such as wing, fuselage, and empennage were based on the fully stressed design (FSD) method.[34] The FSD optimality[35] means that each member of the structure for the optimal design is fully stressed by at least one of the design load conditions considered. The FSD method is applied to structures that are subject to only stress and minimum gage constraints.

In addition to the FSD, the stability analysis such as buckling and crippling is performed for beam and shell elements in this study. The critical buckling stress of beam structure is calculated using Euler buckling equation. For shell structure including skin, spar, and rib, analytic buckling equation is also utilized, which is extended from 1-D Euler buckling equation. For crippling analysis, two semi-empirical methods based on a great deal of experiments data are available: Needham method and Gerard method. Furthermore, a local post-buckling analysis is also addressed considering the effective width for the stringer design.

3.2 Buckling Criteria

3.2.1 Column Buckling

The column is the simplest structural member that is subject to the instability due to compressive load and/or shear flow. A perfectly straight and untwisted column bears an increasing load up to the critical load, P_{cr} , if the load is centrally imposed on the column. The critical buckling load of column can be calculated using the Euler buckling equation as in Equation (3.1).[36]

$$P_{cr} = \frac{\pi^2 EI}{L^2} \quad (3.1)$$

where F_c : Euler buckling load

E : Modulus of elasticity

I : Moment of inertia for the column cross section

L : Length of the column

Equation (3.1) is valid only in case of a simple pin-ended column because the Euler buckling equation depends on the boundary condition, that is, the end fixity condition, as well as material elastic modulus, moment of inertia, and length of the column. Therefore, the Euler buckling equation can be rewritten as Equation (3.2) in consideration of various end fixity conditions, where L' is the effective length of column including the end restraint effect on rotation. Figure 3.1 represents the column end fixity coefficients under the axial and distributed shear load according to the end fixity conditions.

$$P_{cr} = \frac{\pi^2 EI}{L'^2} \quad (3.2)$$

where c : End fixity coefficient

L' : Effective column length = L/\sqrt{c}

With respect to stress instead of force, Equation 3.2 can be also rewritten by introducing the slenderness ratio term, L'/ρ as Equation (3.3).

$$F_{cr} = \frac{P_{cr}}{A} = \frac{\pi^2 E}{(L'/\rho)^2} \quad (3.3)$$

where c : End fixity coefficient

ρ : Radius of gyration of column cross section ($=\sqrt{I/A}$)

A : Area of column cross section

When the critical stress is beyond the proportional limit, elastic modulus (E) in Equation (3.3) will be replaced with tangent modulus of elasticity (E_t).

Among the structural members of aircraft, the stringer of wing, fuselage, and empennage, and the frame of fuselage are modeled as the column structure using the beam element in FEM. As a design criterion of column buckling, the ratio of the actual one to the critical stress, as shown in Equation (3.4), is checked during the optimization process.

$$\frac{F}{F_{cr}} - 1 \leq 0 \quad (3.4)$$

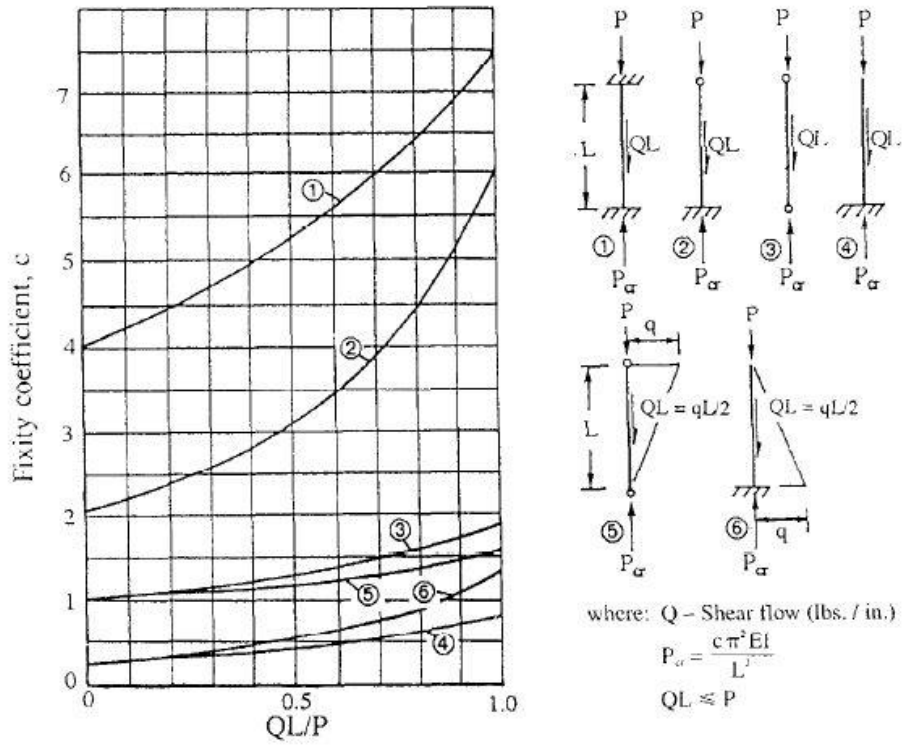


Figure 3.1 Column End Fixity Coefficients [36]

3.2.2 Shell Buckling

The buckling equation for thin sheet is derived from the Euler column buckling equation. In this study, both compression buckling and shear buckling can be considered for the skin, the spar, and the rib design. The corresponding buckling equations are shown in Equations (3.5) and (3.6). [36,37] Figures 3.2 and 3.3 show the buckling coefficient curves for compression and shear load, respectively. [37]

$$\sigma_{cr} = \frac{\pi^2 k_c E}{12(1 - \nu_e^2)} \left(\frac{t}{b}\right)^2 \quad (3.5)$$

where b : Plate length at loaded edge
 E : Modulus of elasticity
 k_c : Compressive buckling coefficient
 ν_e : Poisson's ratio

$$\tau_{cr} = \frac{\pi^2 k_s E}{12(1 - \nu_e^2)} \left(\frac{t}{b}\right)^2 \quad (3.6)$$

where b : Plate length at loaded edge
 E : Modulus of elasticity
 k_s : Shear buckling coefficient
 ν_e : Poisson's ratio

Similar to the column buckling, the ratio of the actual one to the critical stress, as shown in Equation (3.7) and (3.8), is checked during the optimization process. The interaction equation of combined shear and compression is shown in Equation (3.9), while the margin of safety in Equation (3.10).

$$\frac{\sigma}{\sigma_{cr}} - 1 \leq 0 \quad (3.7)$$

$$\frac{\tau}{\tau_{cr}} - 1 \leq 0 \quad (3.8)$$

$$R_L + R_S^2 = 1.0 \quad (3.9)$$

$$M.S. = \frac{2}{\left(R_L + \sqrt{R_L^2 + 4R_S^2}\right)} - 1 \quad (3.10)$$

But, it is uncomfortable and frustrating to find a required value from these coefficient curves in Bruhn[37]. Furthermore, in order to utilize the curves in computer programming, the coefficient curve must be expressed as a function, for example, a polynomial function. Hence, the point data were extracted from the image of coefficient curves using an open source freeware called ‘Engauge Digitizer 5.1’[38], which can convert an image file showing a graph into numbers. Then the point data obtained were transformed to a polynomial function through the simple curve fitting.

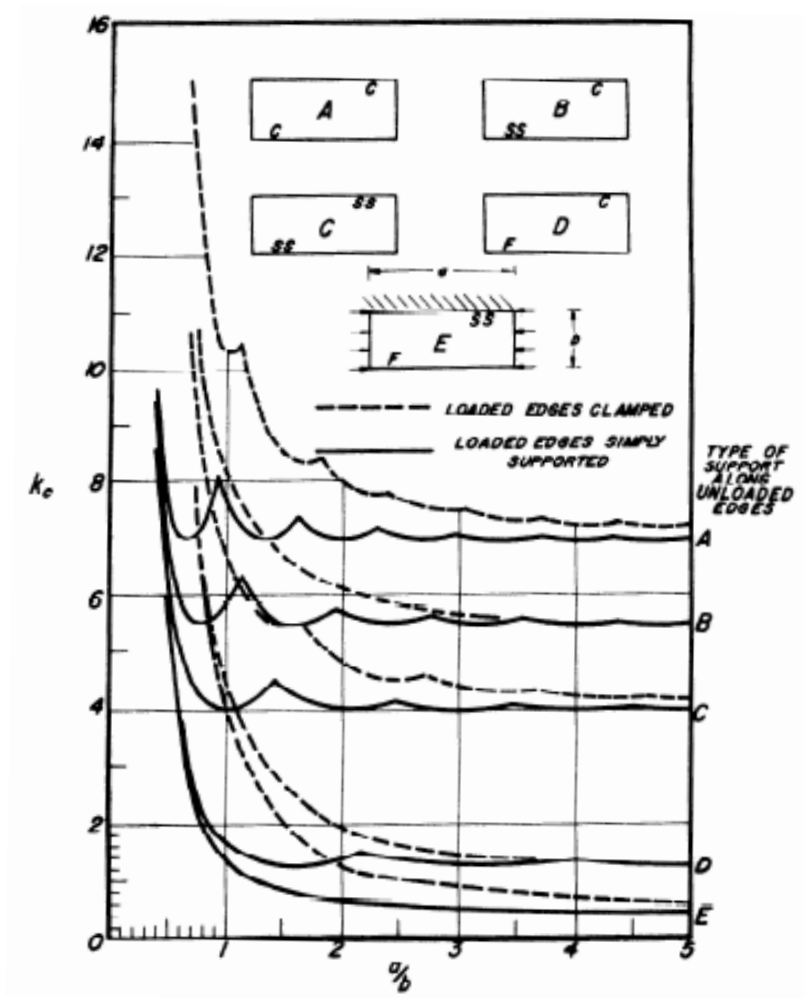


Figure 3.2 Compressive Buckling Coefficients for Flat Rectangular Plates [37]

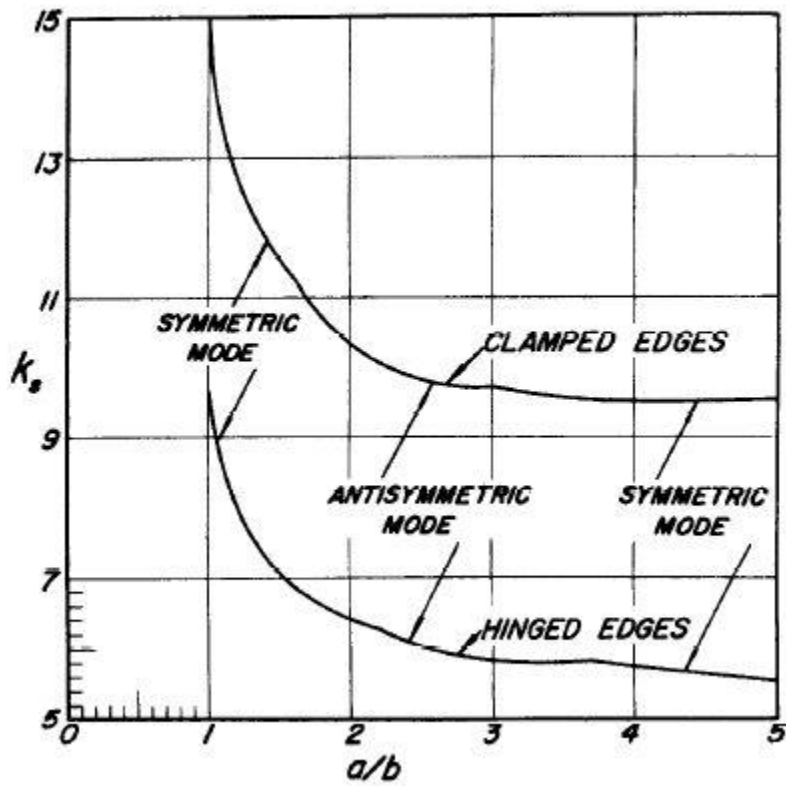


Figure 3.3 Shear Buckling Coefficients for Flat Rectangular Plates [37]

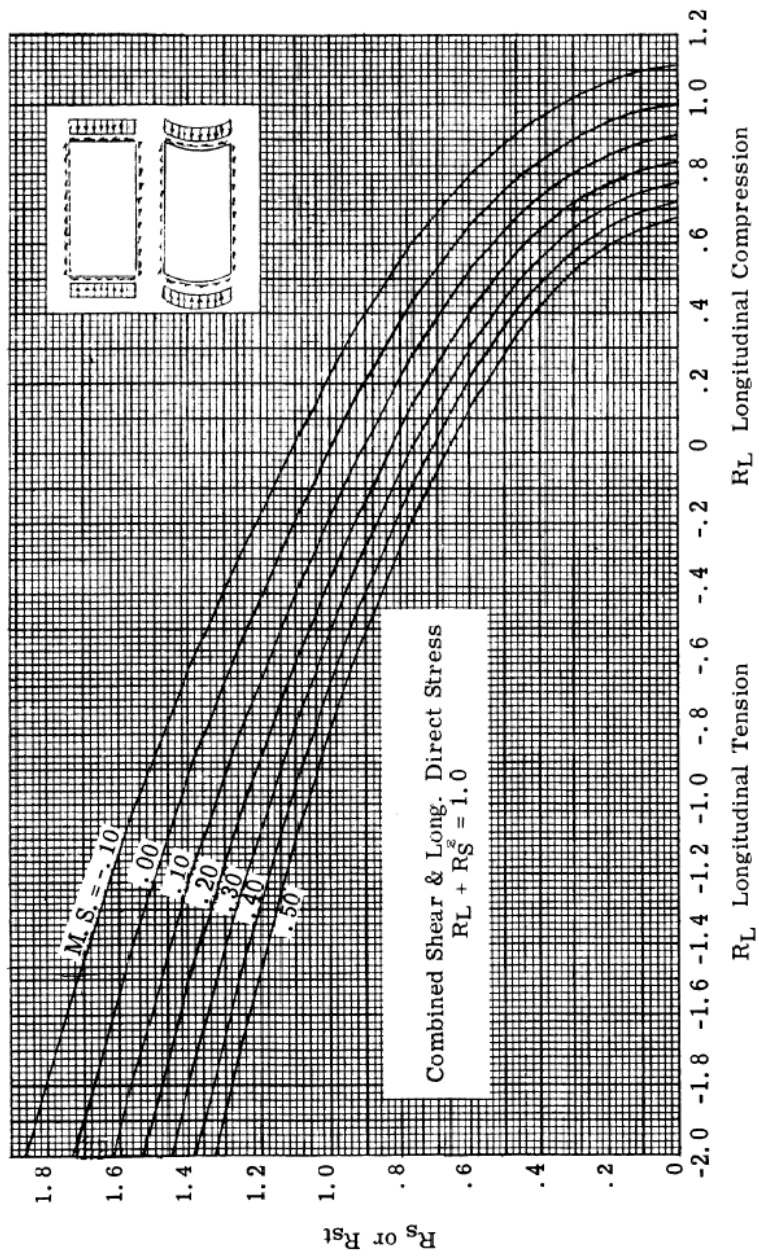


Figure 3.4 Interaction Equation for Combined Shear and Compression [37]

3.3 Crippling Criteria

For the prediction of crippling failure, it is necessary to rely on test results and use empirical methods. Compressive crippling is defined as an inelasticity of the cross section of a structural member in its own plane rather than along its longitudinal axis. [37] It is notable that the maximum crippling stress of a member is a function of its cross section rather than its length. The crippling stress for a given section is calculated with the assumption that the stress is uniform over the entire section although it is actually not uniform. So, parts of the section might buckle at a stress below the crippling stress, and the more stable area such as intersection and corners reach a higher stress than the buckled members as shown in Figure 3.5.

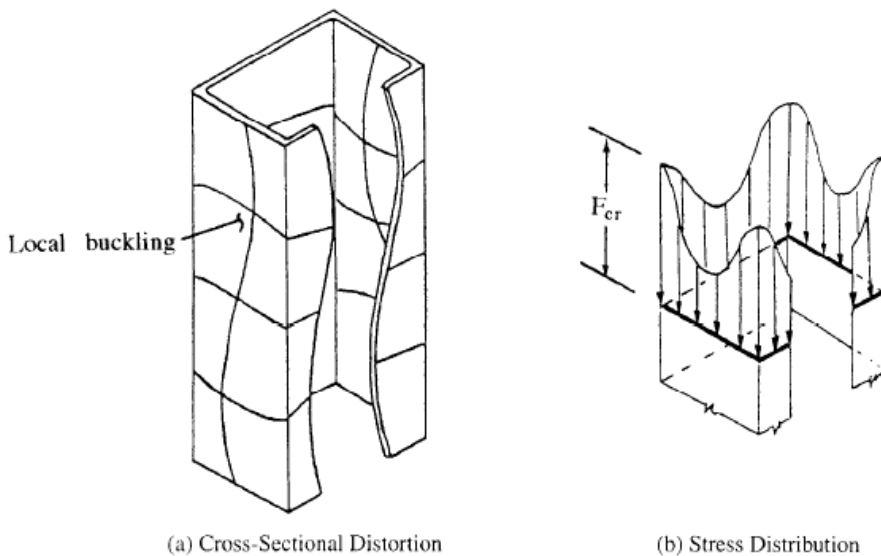


Figure 3.5 Cross Section Subjected to Crippling Stress [36]

DIAMOND/AIRCRAFT provides two methods in order to calculate a crippling stress: Needham method and Gerard method. In Needham method, the member section is broken down into angle units or segments. From a study of test data on various types of cross sections, the following crippling stress equation for angle sections was derived as shown in Equation (3.11).[37] Figure 3.6 represents the curves for determining the crippling stress of angle units in accordance with Equation (3.11).

$$F_{cs}/(F_{cy}E)^{\frac{1}{2}} = C_e/(b'/t)^{0.75} \quad (3.11)$$

where F_{cs} : Crippling stress

F_{cy} : Compression yield stress

E : Modulus of elasticity

b'/t : Equivalent b/t of section = $(a+b)/2t$

C_e : Coefficient that depends on the degree of edge support

Table 3.1 represents the type of basic angle units and each coefficient (C_e) according to edge conditions. The failing strength of angle section can be computed by dividing the section into a series of angle segments and summing the crippling loads for each segment in a weighted average sense as shown in Equation (3.12).[37]

$$F_{cs} = \frac{\Sigma(\text{crippling loads of angles})}{\Sigma(\text{area of angles})} = \frac{\Sigma A_i F_{cs,i}}{\Sigma A_i} \quad (3.12)$$

Gerard method has given more generalized semi-empirical method of determining the crippling stress than Needham method. The Gerard method reflects the distortion effect of the free unloaded edges upon the failing strength of the member section. The crippling equations of Gerard method are shown in Equations (3.13) to (3.15).

For sections with distorted unloaded edges,

$$F_{cs}/F_{cy} = 0.56 \left[(gt^2/A)(E/F_{cy})^{1/2} \right]^{0.85} \quad (3.13)$$

For sections with straight unloaded edges,

$$F_{cs}/F_{cy} = 0.67 \left[(gt^2/A)(E/F_{cy})^{1/2} \right]^{0.40} \quad (3.14)$$

For 2 corner sections,

$$F_{cs}/F_{cy} = 3.2 \left[(t^2/A)(E/F_{cy})^{1/3} \right]^{0.75} \quad (3.15)$$

where F_{cs} : Crippling stress

F_{cy} : Compression yield stress

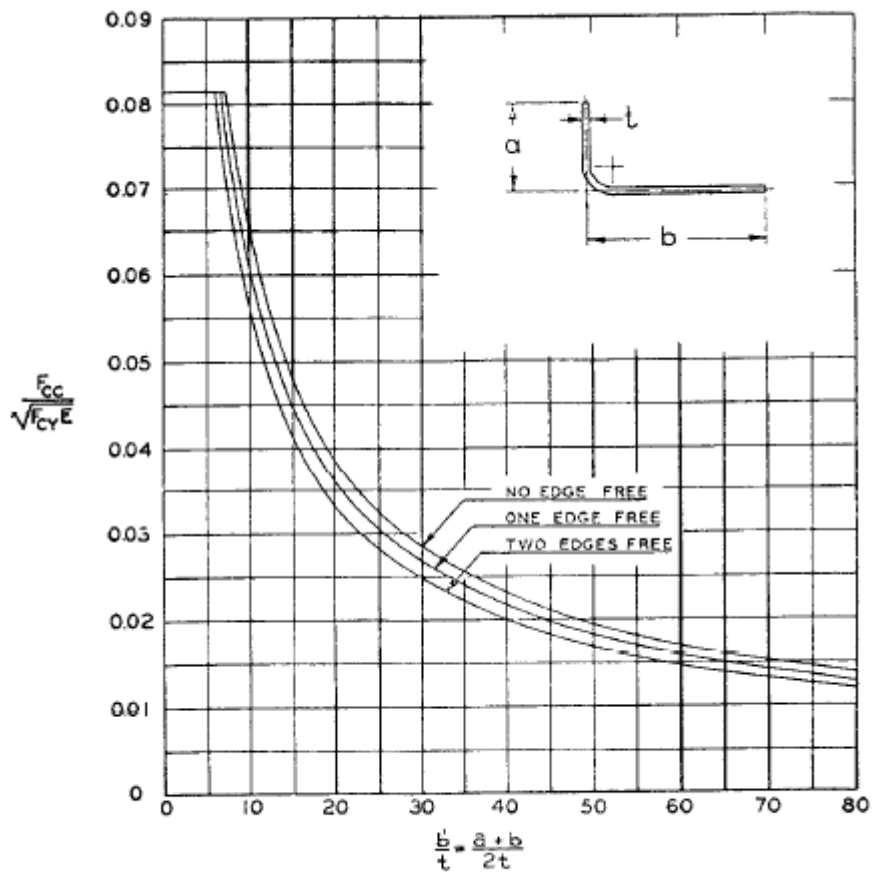
t : Element thickness

E : Modulus of elasticity

A : Section area

g : Number of flanges + number of cuts

In the Equations (3.13) and (3.14), the g value means the number of flanges that make up the section, plus the number of cuts necessary to divide the section into a series of flanges. Table 3.2 summarizes the g value for various cross sections. The maximum crippling stress for a composite section should be limited to the values in Table 3.3 unless test results are obtained to substantiate the use of higher crippling stresses.



(Note: F_{CC} same as F_{CS})

Figure 3.6 Dimensionless Crippling Stress vs. b/t [37]

Table 3.1 Basic Angle Unit for Edge Conditions [37]

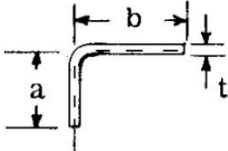
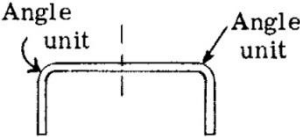
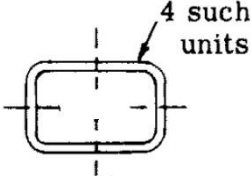
Condition	Shape	C_e
Two edges free	 <p>The diagram shows an L-shaped angle unit. The vertical leg has a height of a, and the horizontal leg has a width of b. The thickness of the legs is t. The unit is shown with dashed lines indicating its position relative to a vertical axis.</p>	0.316
One edge free	 <p>The diagram shows a U-shaped angle unit. Two labels 'Angle unit' with arrows point to the two vertical legs of the U-shape.</p>	0.342
No edge free	 <p>The diagram shows a closed rectangular angle unit, which is a rectangular tube. A label '4 such units' with an arrow points to the top edge of the tube.</p>	0.366

Table 3.2 g values for Various Cross Sections in Gerard Method [36]

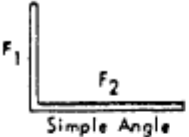
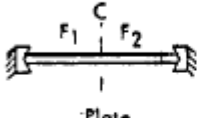
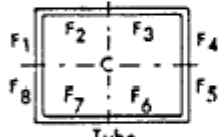
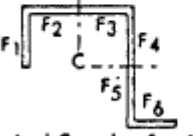
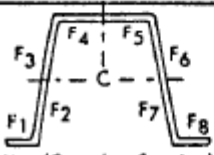
Cross-section	Number of flanges (ΣF)	Number of cuts (ΣC)	$g = F + C$
 <p>Simple Angle</p>	2	0	2
 <p>Plate</p>	2	1	3
 <p>Tube</p>	8	4	12
 <p>Typical Complex Section</p>	6	2	8
 <p>Hat (Complex Section)</p>	8	3	11

Table 3.3 Maximum Values for Crippling Stress [37]

Type of Section	Max. F_{cs}
Angles	$0.7 F_{cy}$
V Groove Plates	F_{cy}
Multi-Corner Sections	$0.8 F_{cy}$
Stiffened Panels	F_{cy}
Tee, Cruciform and H Sections	$0.8 F_{cy}$
2 Corner Sections (Z, J, Channels)	$0.9 F_{cy}$

3.4 Johnson-Euler Interaction Equation

For the column strength of structural members with relatively thick wall thickness, Euler's equation can be used to calculate the critical stress for both elastic and inelastic instability with the tangent modulus E_t used in the inelastic stress range. But the test results for the members with an open cross section, such as channel, hat section, and the like, show that such members with relatively small thickness would follow the path D-E-F-C instead of the path A-B-F-C in Figure 3.7. In other words, the actual critical stress in the path D-E-F is less than that from Euler's equation. The elastic buckling of some part of the cross section begins to initiate at the point F, and then the failure for the member involves both elastic buckling and crippling in the path E-F, which is called *the transition region*. Johnson-Euler equation in Equation (3.16) can be used to calculate the column critical stress in the transition region.[37]

$$F_c = F_{cs} - \frac{F_{cs}^2}{4\pi^2 E} (L'/\rho)^2 \quad (3.15)$$

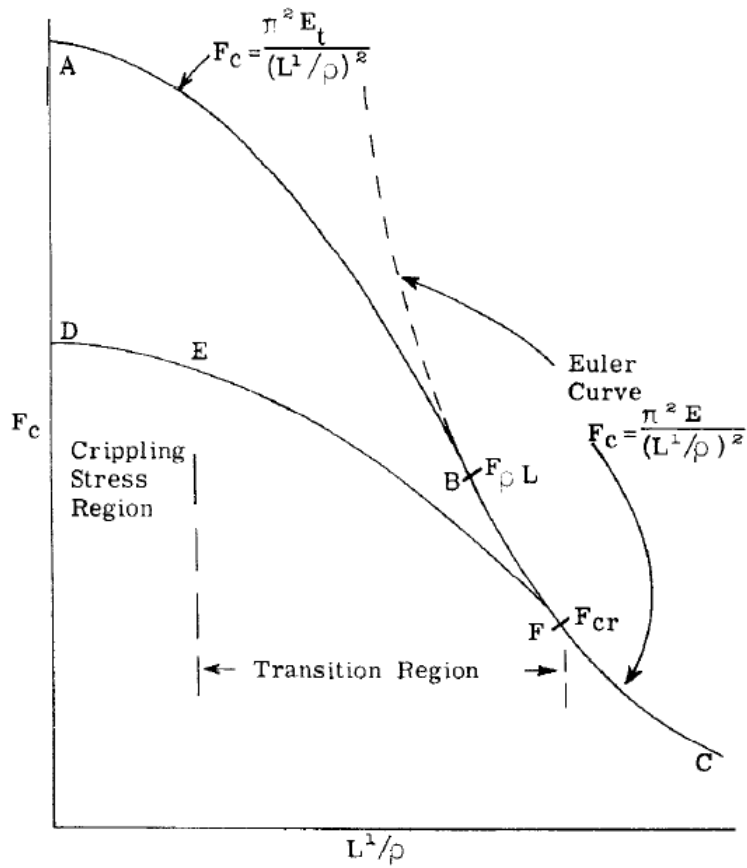


Figure 3.7 Johnson-Euler Interaction Curve [37]

3.5 Material Strength

Material strength criteria is applied using Equation (3.16). For the fatigue dominant structure such as lower skin of wing, it is important that fatigue analysis must be considered with respect to damage tolerant design. In the early design phase, however, the load spectrum for fatigue might not developed. So we instead utilize the ultimate design cut-off stress for damage tolerant design, which is less than static ultimate strength. For example, the ultimate design cut-off stress for Al 2024 is 45,000 psi.[36]

$$\frac{F}{F_c} - 1 \leq 0 \quad (3.16)$$

Chapter 4 Multi-level Optimization

4.1 Overview

The feature of structural design of aircraft with a complex layout leads to a huge-sized mathematical problem with a great deal of design variables accordingly. Hence, the multi-level optimization approach is adequate to solving such a large-scale problem efficiently, where the original problem in the global level can be divided into a set of small subproblems in the local level to be more easily solved.[39,40]

First, at the global level, FE analysis of whole structure is performed in order to calculate internal forces which are required for the evaluation of structural integrity at local level. In the second step, local design variables such as dimensions of stringer and thicknesses of skin and rib are optimized in consideration of design criteria for beam and shell structures. In addition, local post-buckling instability is also investigated for skin-stringer structures. At the moment, aforementioned design criteria play a major role as constraints in optimization process. Then the design variables optimized in the local level are provided to the global level in order to re-calculate internal forces and effective width for the next iteration in the local level. Such a sequential scheme mentioned earlier is repeated as shown in Figure 4.1 until all convergence conditions are satisfied. As optimization algorithm, augmented Lagrangian method (ALM) is employed, which is known to be useful for handling design constraints for efficient computations.

4.2 Literature Survey

In order to design and analyze a complex aerospace structure using numerical modeling, enormous computational resources are required because such a structure have a great deal of design variables for design engineers to define its geometry. Generally, the amount of computational resources required is proportional to the size of numerical problem in question. Furthermore, the direct solution of a large-scale problem would frequently bring about the performance problem such as a poor convergence. In this case, one of the solutions is to break down a large-scale optimization problem into a series of smaller subproblems. Such uncoupled subproblems can be efficiently processed using parallel computing technique which is widely used for aerospace research in recent years. To decompose a large-scale problem into smaller problems is prevalent in MDO for the development of aerospace vehicles. During the development, a lot of disciplines would cooperate with each other, while each discipline preserves its own autonomy from other disciplines in order to concentrate on the specific area of expertise.

Stimulated by the need to decompose the large task into smaller tasks that can be performed in parallel, many decomposition schemes and associated optimization procedures have been proposed until now. Decomposition approach generally not only reduces total computational cost but also generates smaller tasks that are adequate to concurrent operations. Sobieszczanski-Sobieski developed a procedure called the concurrent subspace optimization (CSSO). [41] It allocates the design variables uniquely to subspaces that correspond to subsystems. A separate optimization is

performed within each subspace with respect to its own design variables. But, the application without move limits may cause the convergence problem. [42] Kroo and his colleagues [43–45] proposed another procedure that is known as collaborative optimization (CO). Since then, many other researchers have developed variants of CO and applied it to a number of various design problems. Braun et al. [45] applied this approach to the design of space launch vehicles, and Sobieski and Kroo [46] applied it to the aircraft configuration design. These MDO schemes mentioned above can be adapted to multi-level structural optimization by substituting a module or a discipline with a substructure.

Researchers including Schmit and Sobieszczanski-Sobieski had carried out early researches for multi-level formulations. [47–50] Schmit and Ramanathan [47] presented a multi-level approach for minimum weight structural design of truss and wing structures in consideration of local and system buckling constraints. The optimal design of structure is achieved in the system level subject to strength, displacement, and system buckling constraints, while the component design is performed in the component level satisfying local buckling constraints. Their key idea is to select the objective function in the component level in order to minimize disturbance of loading in the component level due to component level synthesis. Sobieszczanski-Sobieski and Loendorf [49] developed a mixed-optimization method combining mathematical programming to relatively small components and FSD for large structural assemblies of aircraft fuselage. Sobieszczanski-Sobieski et al. [50] proposed a more general multi-level approach. They

proposed a method for decomposing an original problem into a set of subproblems and a coordination problem that preserves coupling between subproblems. They used a cumulative measure of the constraint violation as a function of element forces and stiffness. Sobieszczanski-Sobieski [51] also developed a new method for two-level structural optimization called BLISS/S. In the substructure optimization, local cross sections are optimized as design variables under the highly nonlinear local constraints of strength and buckling, while the global design variables govern the overall structure shape under the displacement constraints.

Based on the multi-level optimization schemes mentioned earlier, many practical researches for industrial application have been also carried out. Williams et al. [52] developed the program for exact vibration and buckling analysis/design called VICONOPT that incorporates the earlier program VIPASA[53] and VICON[54]. In VICONOPT, Lagrange multipliers are used to minimize the total energy of the panel subject to constraints. Bushnell [55–57] developed the program PANDA2, for the design analysis of flat or curved laminated composite panels. Discretized models of panel cross-sections are applied to calculate local and global buckling loads. Carrera et al. [58] developed the two-level optimization tool called NPAO using NASTRAN and PANDA2 for the design of CRV (Crew Return Vehicle), where NASTRAN is used to calculate the loads acting on the panel and the panels are optimized using PANDA2. The optimal solution is obtained taking into account buckling and local post-buckling constraints using NPAO. Bindolino et al. [18] proposed multi-level structural optimization method with

three levels in order to estimate the weight of wingbox of a commercial aircraft through physics-based approach. In the first level, beam model is used to optimize the global behavior of the wing. The optimization for cross section is performed for sizing structural members and selecting a topology of cross section among four models. In the third level, 3-D FE model is generated by means of data from previous levels. The constraints for stress, displacement, and flutter behavior are applied. Dorbath et al. [20] introduced a design tool for wing mass estimation. They extend the structural model beyond the primary structure. ELWIS (finite ELment WIng Structure) is used as the central model generator. Structural analysis and sizing are carried out using the module called Sizing Robot+. The xml-based DLR data model CPACS (Common Parametric Aircraft Configuration Scheme) is used as input and output format.

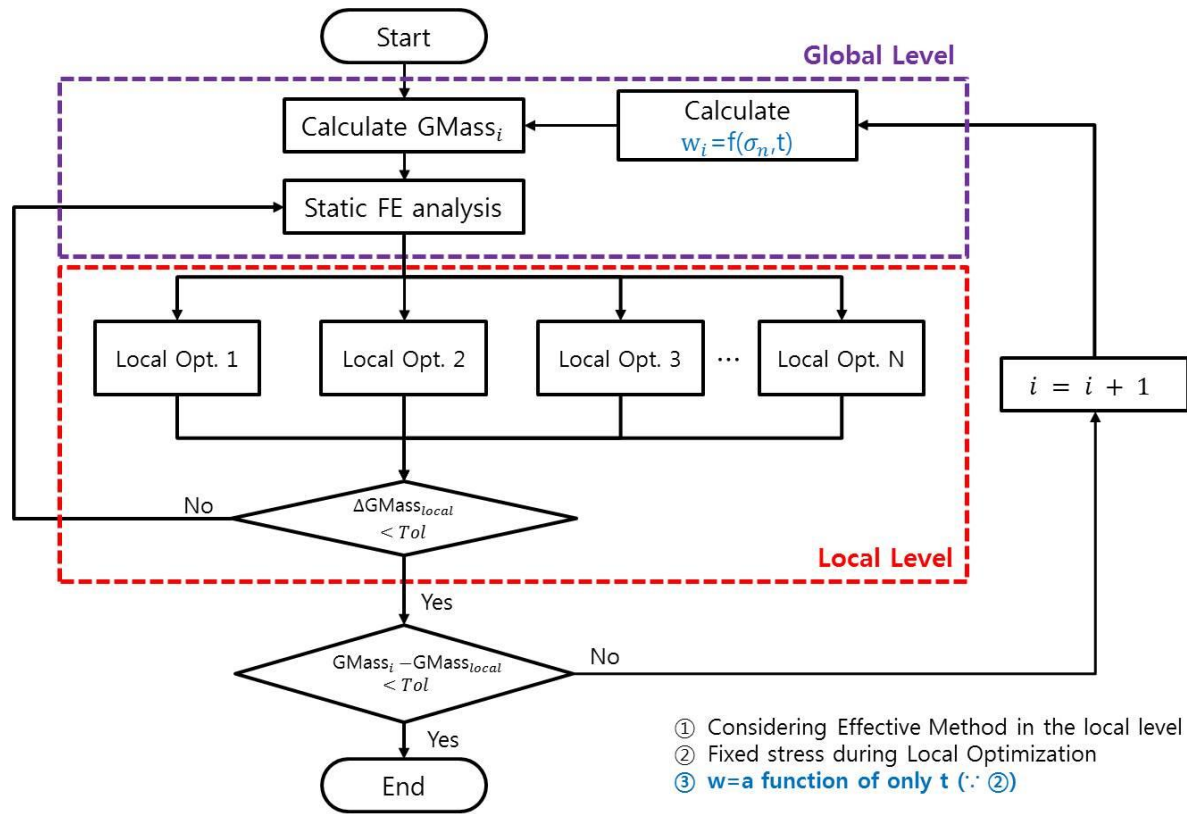


Figure 4.1 Flow Chart for Multi-level Optimization

4.3 Global Level vs. Local Level in MLO

The problem statement of general optimization with both equality and inequality constraints is casted as the following form:

$$\begin{aligned} \min_x f(x) & \quad (4.1) \\ \text{Subject to } h(x) = 0, g(x) \leq 0 \\ \text{where } x \in \mathbb{R}^n, f: \mathbb{R}^n \rightarrow \mathbb{R}, h: \mathbb{R}^n \rightarrow \mathbb{R}^m, g: \mathbb{R}^n \rightarrow \mathbb{R}^r \end{aligned}$$

The design optimization of aircraft structures generally requires lots of consideration about complicated and interactive phenomena related to different disciplines, at least structural mechanics and aerodynamics. Thus it is not tractable to handle a big problem of the whole structure with a large number of DOFs at the same time with respect to computational efficiency and required resources, especially for optimization that requires a number of iterations. In this case, multi-level optimization approach is quite adequate in order to reduce time and cost for computation, which can replace the original problem with multi-level problem in order to solve a set of smaller problems. For aircraft wing, for example, the global problem is for the whole wing structure, and the local problem is for a part of wing, the stiffened panel with skin and stringers. The local-level optimization is performed through bay-by-bay analysis. Each bay is bounded between two adjacent ribs. The skin in local system is bounded in front and rear spars along the chord-wise direction and between two ribs along the span-wise direction, as shown in Figure 4.2.

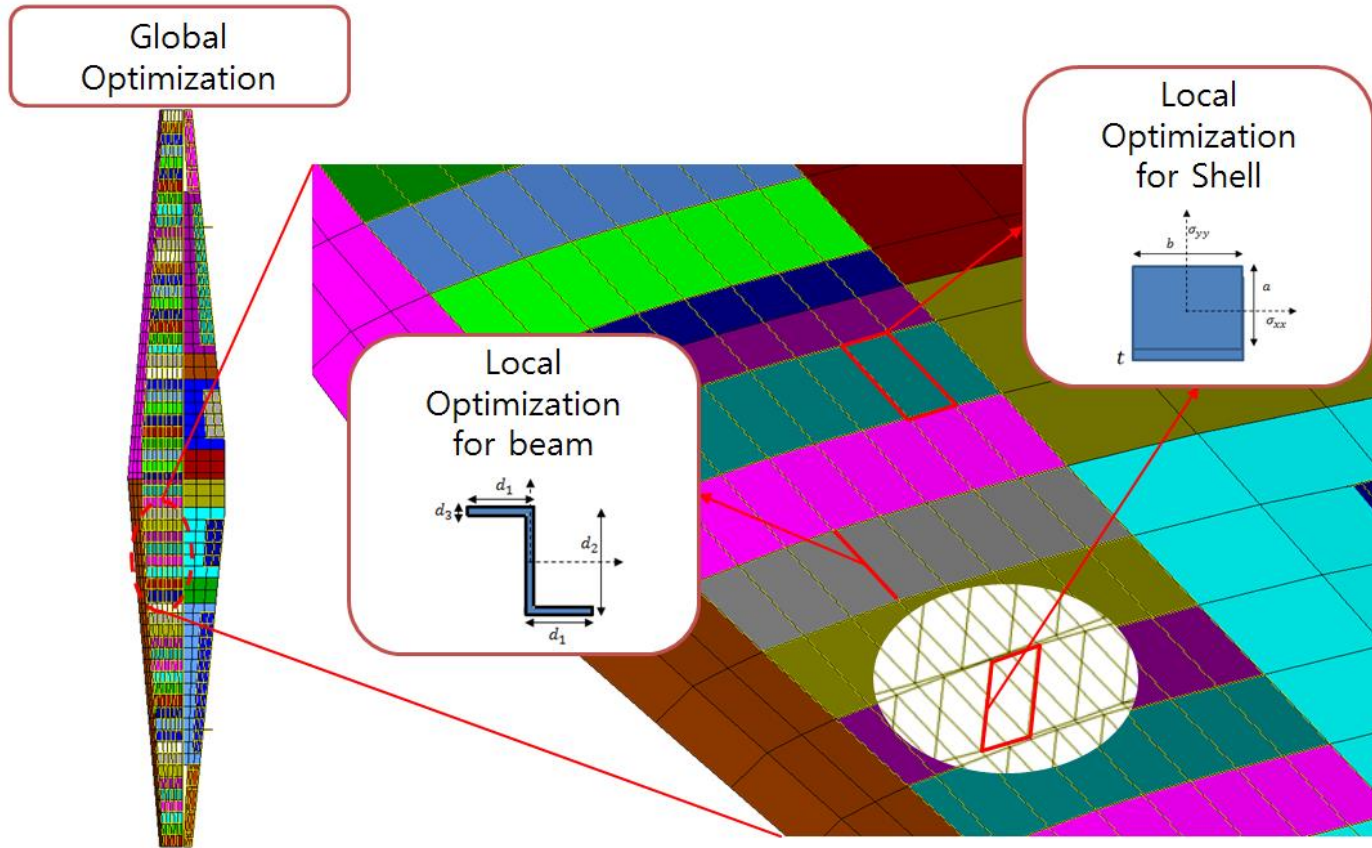


Figure 4.2 Global Level and Local Level in MLO

4.4 Augmented Lagrangian Method

4.4.1 Mathematical Formulation

The original problem for constrained optimization can be transformed into an unconstrained problem with approximation. With respect to mathematical optimization, relaxation is one of approximation strategy, that is, a substitution of a difficult original problem with an approximated problem which can be more easily solved. The constraint functions are added to the objective function as penalized terms instead of applying the strict constraints in the optimization. A solution of the relaxed problem provides information on the original problem. It was already proven that it is optimal for the original problem if an optimal solution for the relaxed problem is feasible for the original problem.

Generally, the quadratic penalty method is one of the most popular approaches, which adds the squares of the constraint violations to the original objective. This approach is widely used in engineering field due to its simplicity but has ill-conditioning characteristics inherently.[59] In this study, Augmented Lagrangian Method (ALM)[59–61] is utilized in order to solve the optimization problem. The ALM is different from the quadratic penalty method in that it avoids the possibility of ill-conditioning by introducing additional Lagrangian multiplier term into the objective function, while it is similar to the quadratic penalty method in that the constrained problem can be replaced with a sequence of unconstrained problems. Unlike the penalty, the augmented Lagrangian function generally keeps smoothness.

We begin with the following Equation (4.2) resulted from Equation (4.1) with both equality and inequality constraints. A vector of additional slack variables z are introduced to transform inequality constraints into equality ones.

$$\min_x f(x) \quad (4.2)$$

$$\text{Subject to } h_1(x) = \dots = h_m(x) = 0,$$

$$g_1(x) + z_1^2 = \dots = g_r(x) + z_r^2 = 0$$

$$\text{where } x \in \mathbb{R}^n, f: \mathbb{R}^n \rightarrow \mathbb{R}, h: \mathbb{R}^n \rightarrow \mathbb{R}^m, g: \mathbb{R}^n \rightarrow \mathbb{R}^r$$

First, the augmented Lagrangian for Equation (4.2) is as follows:

$$\begin{aligned} \bar{L}_A(x, z, \lambda, \mu) = & f(x) + \lambda'h(x) + \frac{1}{2}c|h(x)|^2 \\ & + \sum_{j=1}^r \{\mu_j[g_j(x) + z_j^2] + \frac{1}{2}c|g_j(x) + z_j^2|^2\} \end{aligned} \quad (4.3)$$

Here, we should minimize the augmented Lagrangian, in Equation (4.3) with respect to (x, z) for various multipliers, λ and μ , and penalty parameter c . Equation (4.4) can be written because the minimization of Equation (4.3) can be performed explicitly for each fixed x . Then, the minimization of Equation (4.4) with respect to z is equivalent to Equation (4.5) which is expressed in the quadratic form of u_j representing the square of z_j .

$$\begin{aligned} \min_z \bar{L}_A(x, z, \mu) = & f(x) + \lambda'h(x) + \frac{1}{2}c|h(x)|^2 \\ & + \sum_{j=1}^r \min_{z_j} \{\mu_j[g_j(x) + z_j^2] + \frac{1}{2}c|g_j(x) + z_j^2|^2\} \end{aligned} \quad (4.4)$$

$$\min_{u_j \geq 0} \{\mu_j[g_j(x) + u_j] + \frac{1}{2}c|g_j(x) + u_j|^2\} \quad (4.5)$$

Differentiating Equation (4.5) with respect to u_j and then substituting u_j with \hat{u}_j at which the derivative is zero, we finally obtain Equation (4.6).

$$\hat{u}_j = -[(\mu_j/c) + g_j(x)] \quad (4.6)$$

Because \hat{u}_j must be either $\hat{u}_j \geq 0$ by which Equation (4.5) is solved or equal to zero, the solution of Equation (4.5) can be written as Equation (4.7).

$$u_j^* = \max\{0, -[(\mu_j/c) + g_j(x)]\} \quad (4.7)$$

In order to express Equation (4.3) in a simple form, we define the notation g_j^+ as follows:

$$g_j(x) + u_j^* = \max\{g_j(x), -(\mu_j/c)\} \equiv g_j^+(x, \mu_j, c) \quad (4.8)$$

$$g^+(x, \mu, c) = \begin{bmatrix} g_1^+(x, \mu_1, c) \\ \vdots \\ g_r^+(x, \mu_r, c) \end{bmatrix} \quad (4.9)$$

With Equations (4.4)-(4.9), Equation (4.3) can be arranged as the following equation (4.10).

$$\begin{aligned} \min_z \bar{L}_A(x, z, \lambda, \mu) = & f(x) + \lambda' h(x) + \frac{1}{2} c |h(x)|^2 \\ & + \mu' g^+(x, \mu, c) + \frac{1}{2} c |g^+(x, \mu, c)|^2 \end{aligned} \quad (4.10)$$

Finally, the augmented Lagrangian can be expressed as Equation (4.11) because it is not the function of the slack variable z any longer.

$$\begin{aligned} L_A(x, \lambda, \mu) = & f(x) + \lambda' h(x) + \mu' g^+(x, \mu, c) \\ & + \frac{1}{2} c \{|h(x)|^2 + |g^+(x, \mu, c)|^2\} \end{aligned} \quad (4.11)$$

During iterations, Equation (4.11) is solved approximately and then the Lagrange multipliers and the penalty parameter are updated according to Equations (4.12) to (4.14), where the superscript k represents k -th iteration. In this study, we use $\alpha=1.1$ as the coefficient for updating the penalty parameter.

$$\lambda_j^{k+1} = \lambda_j^k + c^k h(x^k) \quad (4.12)$$

$$\mu_j^{k+1} = \mu_j^k + g_j^+(x^k, \mu_j^k, c^k) = \mu_j^k + \max\{g_j(x), -(\mu_j/c)\} \quad (4.13)$$

$$c^{k+1} = \alpha c^k, \quad \alpha > 1 \quad (4.14)$$

Figures 4.3 and 4.4 show the flow charts of augmented Lagrangian method and Newton method, respectively. In ALM code, Newton method is utilized to find a search direction during the optimization, where the gradient and hessian of constraint functions are calculated.

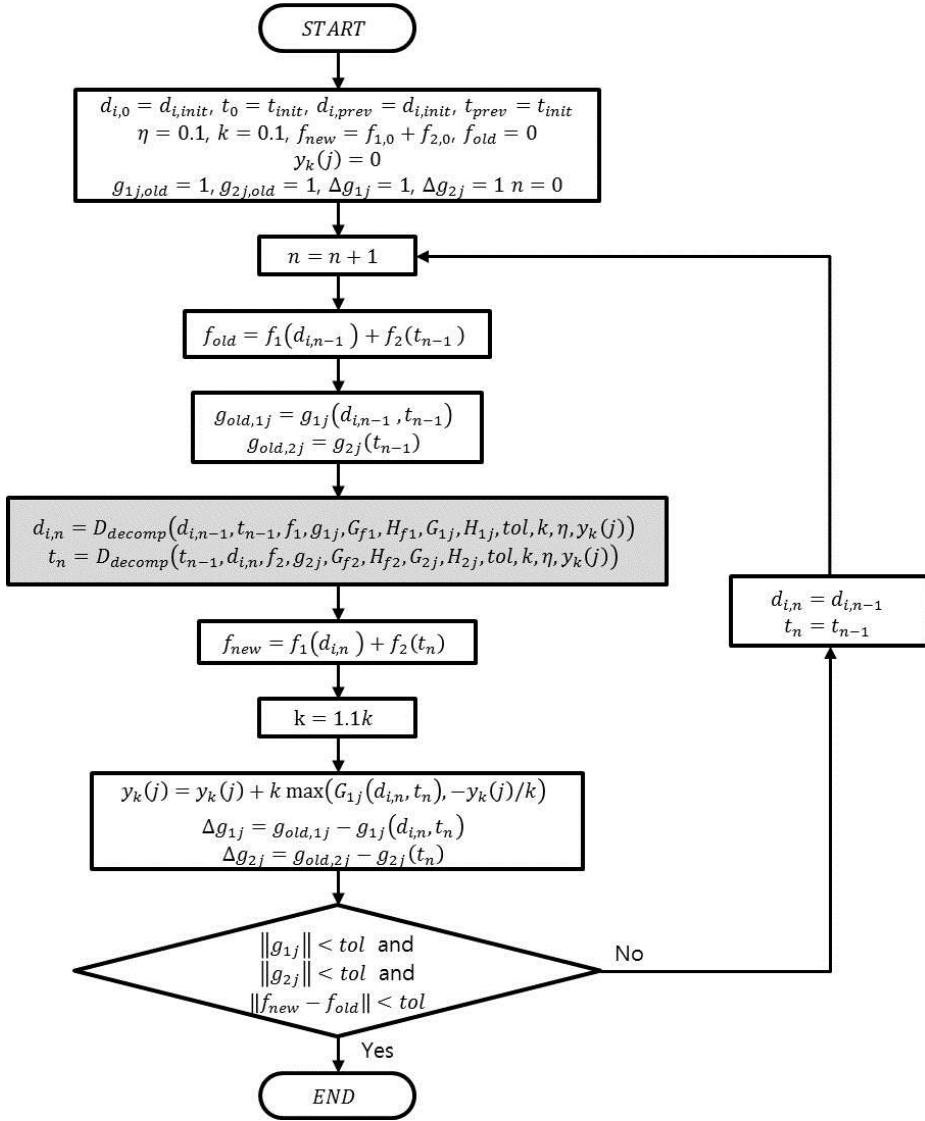


Figure 4.3 Flowchart of Augmented Lagrangian Method (ALM)

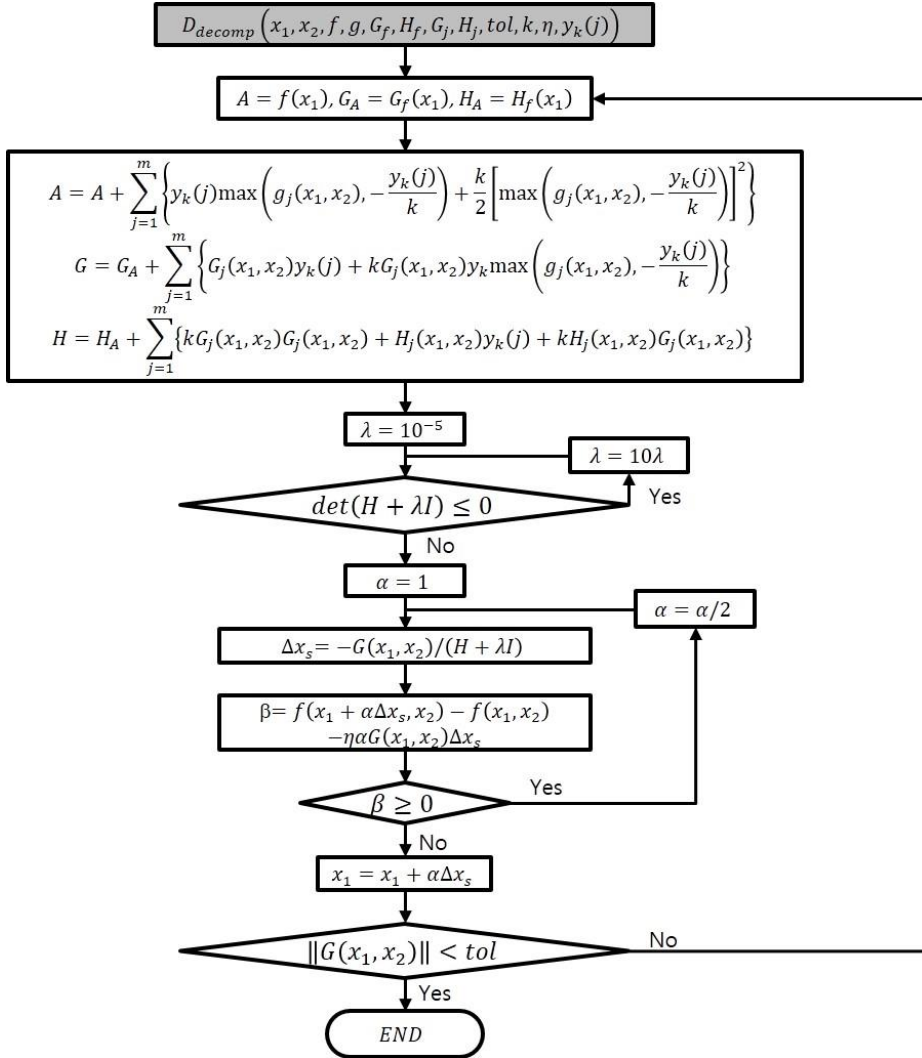


Figure 4.4 Flowchart of Newton Method in ALM

4.4.2 Test Problem for Code Validation

In order to validate the code for ALM formulated in the previous part, the following optimization problem is introduced and solved with the code.

$$\min_{x,y \geq 0} f(x,y) = -x_1 - x_2 - 2y_1 - y_2 \quad (4.15)$$

$$\begin{aligned} \text{Subject to } g_1(x,y) &= x_1 + 2x_2 + 2y_1 + y_2 - 40 \leq 0 \\ g_2(x,y) &= x_1 + 3x_2 \quad \quad \quad - 30 \leq 0 \\ g_3(x,y) &= 2x_1 + x_2 \quad \quad \quad - 20 \leq 0 \\ g_4(x,y) &= \quad \quad \quad y_1 \quad \quad - 10 \leq 0 \\ g_5(x,y) &= \quad \quad \quad y_2 - 10 \leq 0 \\ g_6(x,y) &= \quad \quad \quad y_1 + y_2 - 15 \leq 0 \end{aligned}$$

Equation (4.15) is one of the optimization problem with a coupled constraint as seen in the constraint function g_1 of both x and y . For all variables, four positively bounded constraints are added to the above six constraint functions, and there are totally ten constrains.

$$\begin{aligned} g_7(x,y) &= -x_1 \quad \quad \quad \leq 0 \\ g_8(x,y) &= \quad \quad -x_2 \quad \quad \quad \leq 0 \\ g_9(x,y) &= \quad \quad \quad -y_1 \quad \quad \leq 0 \\ g_{10}(x,y) &= \quad \quad \quad -y_2 \quad \leq 0 \end{aligned}$$

As mentioned earlier, the original constrained problem can be replaced with the unconstrained dual problem which takes the constraints into account by augmenting the objective function with a weighted sum of the constraint functions. Equation (4.15) is transformed into the augmented Lagrangian function in Equation (4.16)

$$\min_{x,y,\mu \geq 0} L_A(x,y,\mu) = f(x,y) + \mu'g^+(x,y,\mu,c) + \frac{1}{2}c|g^+(x,y,\mu,c)|^2 \quad (4.16)$$

The initial values for variables are all zero, that is, $x_1 = x_2 = y_1 = y_2 = 0$. Figures 4.5 and 4.6 show the convergence history of the design variables and the objective function, respectively. Table 4.1 represents the convergence history of the objective function and the constraint functions.

As seen in Figure 4.5, the design variables are converged after 8th iteration. The optimal design point is $(x_1, x_2) = (8.333, 3.333)$ and $(y_1, y_2) = (10, 5)$, and then the optimal value of the objective function is -36.667. According to Figure 4.6, it seems as though the optimal value of the objective function is already found at 2nd iteration. But it is not the optimal because some violations for constraint functions are involved when the constraint functions are checked out. In Table 4.1, the shaded cell represents the violation for any of constraint functions. Eventually, the optimal design point can be obtained at 8th iteration, satisfying all the constraint conditions at the same time.

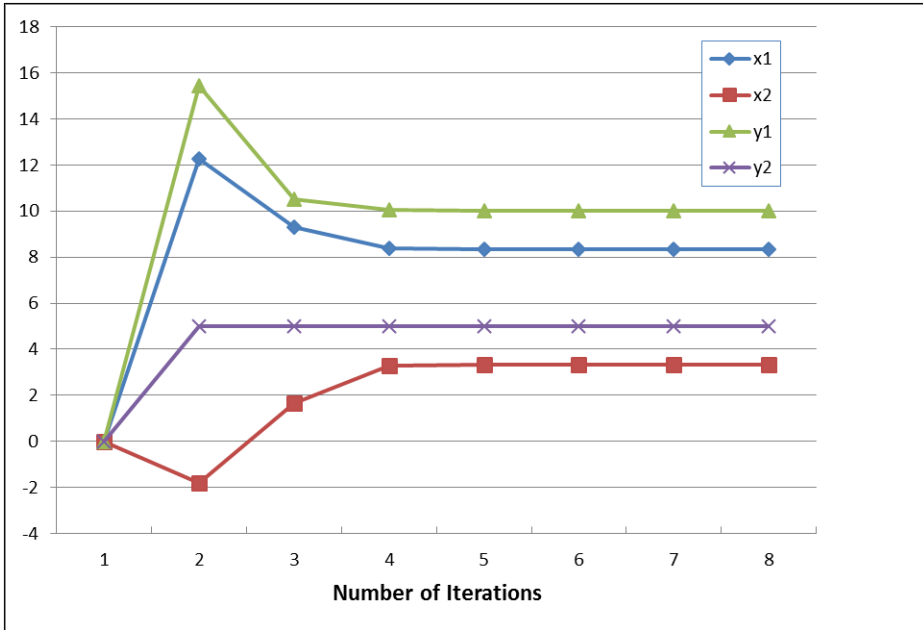


Figure 4.5 Convergence History of Design Variables

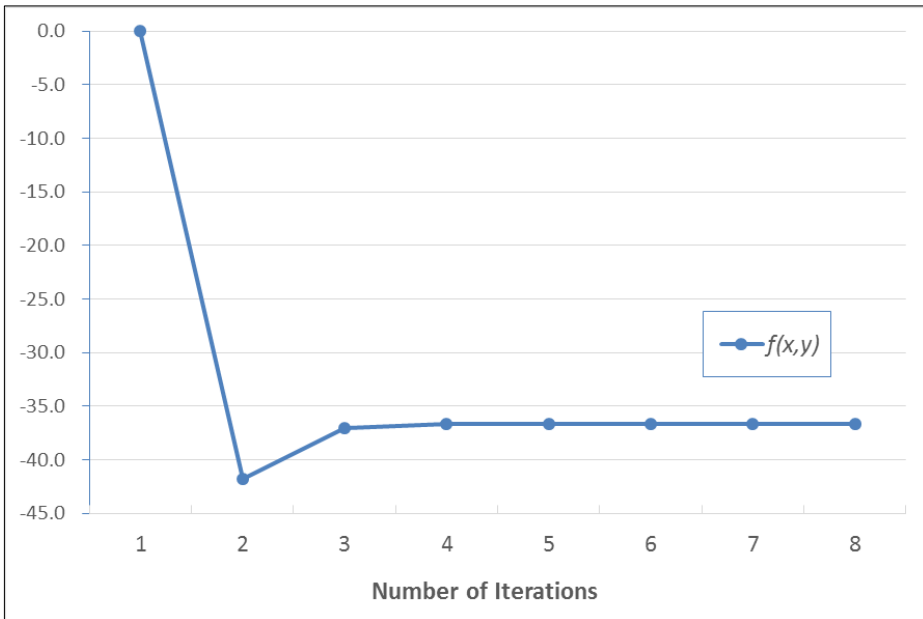


Figure 4.6 Convergence History of Objective Function

Table 4.1 History of Constraint Functions

Number of Iterations	1	2	3	4	5	6	7	8
f	0.000	-41.818	-37.017	-36.667	-36.667	-36.667	-36.667	-36.667
g_1	-40.000	4.546	-1.405	0.028	-0.002	1.400E-4	1.000E-4	0.000
g_2	-30.000	-23.182	-15.744	-11.814	-11.653	-11.668	-11.667	-11.667
g_3	-20.000	2.727	0.248	0.028	-0.002	2.200E-4	0.000	0.000
g_4	-10.000	5.455	0.496	0.055	-0.005	4.000E-4	0.000	0.000
g_5	-10.000	-5.000	-5.000	-5.000	-5.000	-5.000	-5.000	-5.000
g_6	-15.000	5.455	0.496	0.055	-0.005	4.000E-4	0.000	0.000
g_7	0.000	-12.273	-9.298	-8.379	-8.329	-8.334	-8.333	-8.333
g_8	0.000	1.818	-1.653	-3.269	-3.339	-3.333	-3.333	-3.333
g_9	0.000	-15.455	-10.496	-10.055	-9.995	-10.000	-10.000	-10.000
g_{10}	0.000	-5.000	-5.000	-5.000	-5.000	-5.000	-5.000	-5.000

※ The numbers in shaded cells mean the violation of constraint condition because they must be less than or equal to zero.

4.5 Calculation of Gradient and Hessian Matrix

4.5.1 Gradient of Constraint Functions for Beam

The gradient and Hessian matrix of original objective function and constraint functions are calculated in Newton method during the optimization. As mentioned in Chapter 3, the design criteria such as buckling, crippling, material strength, and bounded variables are involved as the constraint functions in the optimization process. Although various types of cross sections can be used in the beam library of DIAMOND/AIRCRAFT, the formulation for the beam with zee-shaped cross section is presented here.

The objective function for beam in a local system is expressed in Equation (4.17), where ρ_m and V represents the material density and the volume of the beam, respectively. Then, the gradient and Hessian matrix can be calculated as Equations (4.18) and (4.19), where only the cross section area is the function of design variables.

$$f_1(x_i) = \rho_m V = \rho_m A(x_i) L \quad (4.17)$$

$$G_{f_1} = \frac{\partial f_1}{\partial x_i} = \rho_m L \frac{\partial A}{\partial x_i} \quad (4.18)$$

$$H_{f_1} = \rho_m L \frac{\partial^2 A}{\partial x_i \partial x_j} = \rho_m L \begin{bmatrix} \frac{\partial^2 A}{\partial x_1 \partial x_1} & \cdots & \frac{\partial^2 A}{\partial x_1 \partial x_n} \\ \vdots & \ddots & \vdots \\ \frac{\partial^2 A}{\partial x_n \partial d_1} & \cdots & \frac{\partial^2 A}{\partial x_n \partial x_n} \end{bmatrix} \quad (4.19)$$

The gradient of constraint functions can be calculated as the following equations.

- Gradient of Crippling Constraint Function

$$G_{11}(i) = \frac{\partial g_{11}}{\partial x_i} = -\frac{\partial \sigma_n}{\partial x_i} - \frac{\partial F_c}{\partial x_i} \quad (\text{if } \sigma_n < 0) \quad (4.20)$$

$$\text{where } \frac{\partial F_c}{\partial x_i} = \left(1 - \frac{F_{cs}}{2\pi^2 E} (L'/\rho)^2\right) \frac{\partial F_{cs}}{\partial x_i} + \frac{(F_{cs}L')^2}{2\pi^2 E \rho^3} \frac{\partial \rho}{\partial x_i}$$

*Derivative of Crippling Stress F_{cs} for z-cross section Beam

$$\begin{aligned} \frac{\partial F_{cs}}{\partial x_1} &= -2.4 F_{cy} (x_3^2/A)^{0.75} (E/F_{cy})^{0.75/2} \frac{1}{A} \frac{\partial A}{\partial x_1} \\ \frac{\partial F_{cs}}{\partial x_2} &= -2.4 F_{cy} (x_3^2/A)^{0.75} (E/F_{cy})^{0.75/2} \frac{1}{A} \frac{\partial A}{\partial x_2} \\ \frac{\partial F_{cs}}{\partial x_3} &= 2.4 F_{cy} (x_3^2/A)^{-0.25} (E/F_{cy})^{0.75/2} \left(\frac{2x_3}{A} - \frac{x_3^2}{A^2} \frac{\partial A}{\partial x_3} \right) \\ \frac{\partial F_{cs}}{\partial t} &= -2.4 F_{cy} (g x_3^2/A)^{0.75} (E/F_{cy})^{0.75/2} \frac{1}{A} \frac{\partial A}{\partial t} \end{aligned} \quad (4.21)$$

- Gradient of Buckling Constraint Function

$$G_{12}(i) = \frac{\partial g_{12}}{\partial x_i} = -\frac{\partial \sigma_n}{\partial x_i} - \frac{\partial F_{cr}}{\partial x_i} \quad (\text{if } \sigma_n < 0) \quad (4.22)$$

$$\text{where } \frac{\partial F_{cr}}{\partial x_i} = \frac{2\pi^2 E \rho}{(L')^2} \frac{\partial \rho}{\partial x_i}$$

- Gradient of Material Strength Constraint Function

$$G_{13}(i) = \frac{\partial g_{13}}{\partial x_i} = \begin{cases} \frac{\partial \sigma_n}{\partial x_i} \leq 0 & (\text{if } \sigma_n > 0) \\ -\frac{\partial \sigma_n}{\partial x_i} \leq 0 & (\text{if } \sigma_n < 0) \end{cases} \quad (4.23)$$

The relation of internal force F_{in} and normal stress σ_n is described as Equation (4.24), and then the partial derivative of internal force with respect to a design variable x_i can be expressed as Equation (4.25). Here, we assume that $\frac{\partial F_{in}}{\partial x_i} = 0$ because there is no internal force update during the optimization in the local level.

$$F_{in} = \sigma_n(x_i) A(x_i) \quad (4.24)$$

$$\frac{\partial F_{in}}{\partial x_i} = \frac{\partial \sigma_n}{\partial x_i} A + \sigma_n \frac{\partial A}{\partial x_i} \approx 0 \quad (4.25)$$

Then the partial derivative of normal stress and radius of gyration with respect to design variable can be expressed as Equations (4.26) and (4.27). The derivatives of normal stress with respect to design variables are summarized in Appendix A for the major cross sections of beam.

$$\frac{\partial \sigma_n}{\partial x_i} = -\frac{\sigma_n}{A} \frac{\partial A}{\partial x_i} \quad (4.26)$$

$$\frac{\partial \rho}{\partial x_i} = \frac{\rho}{2} \left(\frac{1}{I} \frac{\partial I}{\partial x_i} - \frac{1}{A} \frac{\partial A}{\partial x_i} \right) \quad (4.27)$$

4.5.2 Hessian of Constraint Functions for Beam

The Hessian Matrix of constraint functions can be calculated as the following equations.

- Hessian of Crippling Constraint Function

$$H_{11}(i, j) = \frac{\partial^2 g_{11}}{\partial x_i \partial x_j} = -\frac{\partial^2 \sigma_n}{\partial x_i \partial x_j} - \frac{\partial^2 F_c}{\partial x_i \partial x_j} \quad (\text{if } \sigma_n < 0) \quad (4.28)$$

- Hessian of Buckling Constraint Function

$$H_{12}(i, j) = \frac{\partial^2 g_{12}}{\partial x_i \partial x_j} = -\frac{\partial^2 \sigma_n}{\partial x_i \partial x_j} - \frac{\partial^2 F_{cr}}{\partial x_i \partial x_j} \quad (\text{if } \sigma_n < 0) \quad (4.29)$$

- Hessian of Material Strength Constraint Function

$$H_{13}(i, j) = \frac{\partial^2 g_{13}}{\partial x_i \partial x_j} = \begin{cases} \frac{\partial^2 \sigma_n}{\partial x_i \partial x_j} & (\text{if } \sigma_n > 0) \\ -\frac{\partial^2 \sigma_n}{\partial x_i \partial x_j} & (\text{if } \sigma_n < 0) \end{cases} \quad (4.30)$$

Then the second-order partial derivative of normal stress and radius of gyration with respect to design variable can be expressed as Equations (4.31) and (4.32).

$$\frac{\partial^2 \sigma_n}{\partial x_i \partial x_j} = \frac{2\sigma_n}{A^2} \left(\frac{\partial A}{\partial x_i} \right) \left(\frac{\partial A}{\partial x_j} \right) - \frac{\sigma_n}{A} \frac{\partial^2 A}{\partial x_i \partial x_j} \quad (4.31)$$

$$\begin{aligned} \frac{\partial^2 \rho}{\partial x_i \partial x_j} &= \frac{1}{2} \frac{\partial A}{\partial x_j} \left(\frac{1}{I} \frac{\partial I}{\partial x_i} - \frac{1}{A} \frac{\partial A}{\partial x_i} \right) \\ &+ \frac{\rho}{2} \left\{ -\frac{1}{I^2} \left(\frac{\partial I}{\partial x_i} \right) \left(\frac{\partial I}{\partial x_j} \right) + \frac{1}{I} \frac{\partial^2 I}{\partial x_i \partial x_j} + \frac{1}{A^2} \left(\frac{\partial A}{\partial x_i} \right) \left(\frac{\partial A}{\partial x_j} \right) - \frac{1}{A} \frac{\partial^2 A}{\partial x_i \partial x_j} \right\} \end{aligned} \quad (4.32)$$

4.5.3 Gradient of Constraint Functions for Shell

The objective function for shell in a local system is expressed in Equation (4.33), where ρ_m and V represent the material density and the volume of the beam, respectively. The area of shell element is the function of ‘ a ’ and ‘ b ’, where ‘ a ’ and ‘ b ’ represent the width along the x -direction and the height along the y -direction. But, both of the width and the height of shell are fixed because they are not considered design variables. Thickness of shell is the only design variable. Then, the gradient and Hessian matrix can be calculated as Equations (4.34) and (4.35), where only the cross section area is the function of design variables. Similar to Equation (4.26) for the beam, Equation (4.36) is derived for the shell.

$$f_2(t) = \rho_m V(a, b, t) = \rho_m A(a, b)t \quad (4.33)$$

$$G_{f_2} = \frac{\partial f_2}{\partial t} = \rho_m A \quad (4.34)$$

$$H_{f_2} = 0 \quad (4.35)$$

$$\frac{\partial \sigma_{mn}}{\partial t} = -\frac{\sigma_{mn}(t)}{t} \quad (4.36)$$

For shell buckling, three kinds of constraint functions are considered as mentioned in Equations (3.7) to (3.10) of Chapter 3.2.2: compression buckling, shear buckling, and compression-shear combined buckling. For shell, axial compression buckling is estimated using the stress by the following rule.

$$\sigma_c = \begin{cases} \sigma_{xx} & (\text{if } b > a) \\ \sigma_{yy} & (\text{if } b < a) \end{cases} \quad (4.37)$$

The constraint functions for compression, shear, and compression-shear combined buckling are expressed as the following equations. Equation (4.40) for the combined buckling is derived from Equation (3.9).

$$g_{21}^{(c)}(t) = -\sigma_c - \sigma_{cr} \leq 0, \quad \text{where } \sigma_{cr} = \frac{\pi^2 k_c E}{12(1 - \nu_e^2)} \left(\frac{t}{b}\right)^2 \quad (4.38)$$

$$g_{21}^{(s)}(t) = -\tau - \tau_{cr} \leq 0, \quad \text{where } \tau_{cr} = \frac{\pi^2 k_s E}{12(1 - \nu_e^2)} \left(\frac{t}{b}\right)^2 \quad (4.39)$$

$$g_{21}^{(com)}(t) = \sigma_{cr} \tau^2 - \sigma_c \tau_{cr}^2 - \sigma_{cr} \tau_{cr}^2 \leq 0 \quad (4.40)$$

The gradient of constraint functions can be calculated using the following equations. But, the shell buckling equation is not used as the constraint condition during the optimization because shell buckling is allowed if the effective width method is considered.

- Gradient of Combined Buckling Constraint Function

$$\begin{aligned} G_{21}^{(comb)} &= \frac{\partial g_{21}^{(c)}}{\partial t} \\ &= \frac{\partial \sigma_{cr}}{\partial t} \tau^2 + 2\sigma_{cr} \tau \frac{\partial \tau}{\partial t} - \frac{\partial \sigma_c}{\partial t} \tau_{cr}^2 - 2\sigma_c \tau_{cr} \frac{\partial \tau_{cr}}{\partial t} \\ &\quad - \frac{\partial \sigma_{cr}}{\partial t} \tau_{cr}^2 - 2\sigma_{cr} \tau_{cr} \frac{\partial \tau_{cr}}{\partial t} \end{aligned} \quad (4.41)$$

Substituting $\tau_{cr} = \left(\frac{k_s}{k_c}\right) \sigma_{cr}$ and $\frac{\partial \tau_{cr}}{\partial t} = \left(\frac{k_s}{k_c}\right) \frac{\partial \sigma_{cr}}{\partial t}$ into (5.29),

$$\begin{aligned} G_{21}^{(comb)} &= \frac{\partial \sigma_{cr}}{\partial t} \tau^2 + 2\sigma_{cr} \tau \frac{\partial \tau}{\partial t} \\ &\quad - \left(\frac{k_s}{k_c}\right)^2 \left\{ \frac{\partial \sigma_c}{\partial t} \sigma_{cr}^2 + 2\sigma_c \sigma_{cr} \frac{\partial \sigma_{cr}}{\partial t} + 3\sigma_{cr}^2 \frac{\partial \sigma_{cr}}{\partial t} \right\} \end{aligned} \quad (4.42)$$

By Equation (4.36), the derivative function of stress with respect to the skin thickness is arranged as Equation (4.43). The derivative function of compression buckling stress is also calculated from Equations (3.5).

$$\frac{\partial \sigma_c}{\partial t} = -\frac{\sigma_c}{t} \quad (4.43)$$

$$\frac{\partial \sigma_{cr}}{\partial t} = \frac{\pi^2 k_c E t}{6b^2(1 - \nu_e^2)} \quad (4.44)$$

Substituting Equations (5.36) and (5.37) into (5.35),

$$G_{21}^{(comb)} = -\left(\frac{k_s}{k_c}\right)^2 (3k_c^2 C_b^2 t^3 \sigma_c + 6k_c^3 C_b^3 t^5) \quad (4.45)$$

$$\text{where } C_b = \frac{\pi^2 E}{12b^2(1 - \nu_e^2)}$$

- Gradient of Compression Buckling Constraint Function

$$G_{21}^{(c)} = \frac{\partial g_{21}^{(c)}}{\partial t} = -\frac{\partial \sigma_c}{\partial t} - \frac{\partial \sigma_{cr}}{\partial t} = -\frac{\sigma_c}{t} - \frac{\pi^2 k_c E t}{6b^2(1 - \nu_e^2)} \quad (4.46)$$

- Gradient of Shear Buckling Constraint Function

$$G_{21}^{(s)} = \frac{\partial g_{21}^{(s)}}{\partial t} = -\frac{\partial \tau}{\partial t} - \frac{\partial \tau_{cr}}{\partial t} = -\frac{\tau}{t} - \frac{\pi^2 k_s E t}{6b^2(1 - \nu_e^2)} \quad (4.47)$$

- Gradient of Material Strength Constraint Function

$$G_{22}^{(mn)} = \frac{\partial g_{22}^{(mn)}}{\partial t} = -\frac{\partial \sigma_{mn}}{\partial t} = -\frac{\sigma_{mn}(t)}{t} \quad (4.48)$$

4.5.4 Hessian of Constraint Functions for Shell

The Hessian Matrix of constraint function can be calculated as the following equation.

- Hessian of Combined Buckling Constraint Function

$$\begin{aligned}
 H_{21}^{(comb)} &= \frac{\partial G_{21}^{(comb)}}{\partial t} \\
 &= -\left(\frac{K_s}{K_c}\right)^2 \left\{ 9K_c^2 C_b^2 t^2 \sigma_c + 3K_c^2 C_b^2 t^3 \frac{\partial \sigma_c}{\partial t} + 30K_c^3 C_b^3 t^4 \right\} \\
 &= -(6K_s^2 C_b^2 t^2 \sigma_c + 30K_s^2 K_c C_b^3 t^4)
 \end{aligned} \tag{4.49}$$

- Hessian of Compression Buckling Constraint Function

$$H_{21}^{(c)} = \frac{\partial G_{21}^{(c)}}{\partial t} = -\frac{\partial \sigma_c}{\partial t} - \frac{\partial \sigma_{cr}}{\partial t} = \frac{2\sigma_c}{t^2} - \frac{\pi^2 k_c E}{6b^2(1-\nu_e^2)} \tag{4.50}$$

- Hessian of Shear Buckling Constraint Function

$$H_{21}^{(s)} = \frac{\partial G_{21}^{(s)}}{\partial t} = -\frac{\partial \tau}{\partial t} - \frac{\partial \tau_{cr}}{\partial t} = \frac{2\tau}{t^2} - \frac{\pi^2 k_s E}{6b^2(1-\nu_e^2)} \tag{4.51}$$

- Hessian of Material Strength Constraint Function

$$H_{22}^{(mn)} = \frac{\partial G_{22}^{(mn)}}{\partial t} = -\frac{\left(\frac{\partial \sigma_{mn}}{\partial t}\right)t - \sigma_{mn}}{t^2} = \frac{2\sigma_{mn}}{t^2} \tag{4.52}$$

Chapter 5 Preliminary Structural Sizing

5.1 Overview

Recently, the 90-seat turboprop market is emerging as a new sector according to the airlines' demand for larger and more cost-efficient turboprop with respect to the growth of traffic volume and the economic requirements, for example, operating cost reduction from fuel efficiency. Currently, the mainstream of turboprop market is 70-seat aircraft such as ATR 72 and Q400. But, it is expected that the 90-seat turboprop will have competitiveness because of push-down from 100-seat aircraft as well as push-up from 50-seat regional jet or 70-seat turboprop deployed when the aspect of fuel economics is underlined. It is worthy of considering such a market trend to determine the type of new aircraft that will be developed. Therefore, the design object in this study is assumed to be a turboprop aircraft which can accommodate 90 passengers on regional flights.

In the following part of this chapter, the preliminary structural design for wing of a transport aircraft will be carried out. The finite element model is generated based on parametric modeling technique, and the structural sizing and the weight estimation are performed using physic-based method, FEM. The general information of turboprop aircraft used in this study was provided by Korea Aerospace Research Institute (KARI), with which this dissertation focuses on the development of design framework and multi-level optimization routine using ALM.

5.2 General Information

5.2.1 Aircraft Configuration

Figure 5.1 shows the configuration of 90-seat turboprop aircraft. According to TRLs, MTOW of the aircraft is about 70,000 pound. The aircraft has two 5,500-SHP turboprop engines for thrust. The landing gears are installed in the nacelle on the wing. As seen in Figure 5.1, the wing is high wing type mounted on the fuselage as the competitor aircrafts. The wing area is 740 ft², and wing span is 94.2 ft. The leading edge of wing has uniform sweepback angle. Figure 5.2 and Table 5.1 show the geometry information of wing. Based on the OML of wing, the internal structural layout is determined later.

5.2.2 Material Selection

In aerospace industry, aluminum alloys are characterized by an excellent strength-to-weight ratio, corrosion resistance, workability or formability, and other predominant characteristics. Among various aluminum alloys, 2000 and 7000 series are the most widely used. The upper skin of wing is made of Al 7150, but the lower skin is made of Al 2024. Al 2024 is generally used for fatigue-critical tension application. The materials of stringers in upper and lower skin are Al 7150 and Al 7075, respectively. Al 7150 is used for high strength major structural applications where weight savings over Al 7075 are required. In addition, the spar and the rib are made of Al 7050. Table 5.2 summarizes the material selection for the structural parts of wing.

Table 5.1 Geometry Information of Wing

Geometry Parameter	Measurement
Wing Span	94.2 ft
Wing Area	740 ft ²
Aspect Ratio	12
Sweepback Angle	5.59° (LE)
Dihedral Angle	2.5°
Taper Ratio	0.35
Mean Aerodynamic Chord (MAC)	101.52

Table 5.2 Material Selection for Wing Component

Structural Component	Material Selection
Upper Skin	Al 7150
Lower Skin	Al 2024
Upper Stringer	Al 7150
Lower Stringer	Al 7075
Spar	Al 7050
Rib	Al 7050

5.3 Problem Statement

In order to find the optimal weight of wing, the global optimization problem is casted as Equation (5.1), where $f_1(x_i^j, u)$ and $f_2(t^k, u)$ represent the weight of beam and shell in a local system, respectively.

$$\min_{x,t} f(x, t, u) = \min_{x,t} \left\{ \sum_{j=1}^{n_b} f_1(x_i^j, u) + \sum_{k=1}^{n_s} f_2(t^k, u) \right\} \quad (5.1)$$

where j = the index of beam element

k : the index of shell element

x_i^j : i -th design variable in j -th beam element

t^k : thickness in k -th shell element

u : global displacement vector

As mentioned in Chapter 4.3, the local level optimization is performed through bay-by-bay analysis. The skin in local system is bounded in front and rear spars along the chord-wise direction and between two ribs along the span-wise direction. Each panel load's derivative with respect to design variable can be assumed to be zero by the assumption that panel loads change slowly during the optimization. As explained in Figure 4.1, stress and displacement are updated in the global level, while they are fixed value in the local level during the optimization. Equation (5.1) can be divided into the objective functions for a set of local systems, which can be solved independently. Then, the local level optimization problem can be arranged as the following Equations (5.2) and (5.3), where σ_n represents the normal stress of beam.

$$\min f_1(x_i) \text{ for beam} \quad (5.2)$$

$$\begin{aligned} \text{Subject to } g_{11}(x_i, u(x_i)) &= -\sigma_n - F_c \leq 0 && \text{(crippling)} \\ g_{12}(x_i, u(x_i)) &= -\sigma_n - F_{cr} \leq 0 && \text{(buckling)} \\ g_{13}(x_i, u(x_i)) &\leq 0 && \text{(material strength)} \\ g_{14}(x_i) &= x_i - x_{i,max} \leq 0 && \text{(upper bound)} \\ g_{15}(x_i) &= x_{i,min} - x_i \leq 0 && \text{(lower bound)} \end{aligned}$$

$$\min f_2(t) \text{ for shell} \quad (5.3)$$

$$\begin{aligned} \text{Subject to } g_{21}(t, u(t)) &\leq 0 && \text{(comp/shear/combined buckling)} \\ g_{22}(t, u(t)) &\leq 0 && \text{(material strength)} \\ g_{23}(t) &= t - t_{max} \leq 0 && \text{(upper bound)} \\ g_{24}(t) &= t_{min} - t \leq 0 && \text{(lower bound)} \end{aligned}$$

Equations (5.2) and (5.3) can be applied to the case in which the effective width is not considered. If the effective width is considered for the panel design, the constraint conditions must be modified. First, among the constraint functions of Equation (5.2), g_{11} and g_{12} become the function of t as well as x_i and u due to the effective width as shown in Equation (5.4).

$$\begin{aligned} g_{11}(x_i, u(x_i), t) &\leq 0 && \text{(crippling)} \\ g_{12}(x_i, u(x_i), t) &\leq 0 && \text{(buckling)} \end{aligned} \quad (5.4)$$

In addition, one of the constraint function, g_{21} , is removed because the skin buckling is allowed when the effective width is considered. In summary, the difference of constraint conditions occurs depending on the consideration of effective width. Later, the change of optimal weights will be presented according to the consideration of effective width.

5.4 Effective Width Method

In Chapter 3.2 to 3.4, the buckling and crippling stresses for column and thin sheet were investigated to apply those stresses to the design criteria for structural sizing, where each member is not fastened to any other adjacent structure. In general, however, the primary structure of aerospace vehicles involves the stiffened panel structure, where thin skin is reinforced by the attached stringers. Since the skin and stringers must deform together, the skin participates in bearing compressive load partly. If such an effect is neglected, it would produce too conservative and undesirable results in the structural design. In order to achieve the goal of weight saving, it is strongly recommended that effective width be considered in the structural design.

Figure 5.3 shows the sheet stress distribution before and after buckling for a continuous flat thin sheet fastened to stiffener. The intact fastened unit is subjected to a uniform compressive load. Once the skin buckles between the stiffeners, the stress distribution is re-arranged, as shown in Figure 5.3, because it is capable of carrying no more stress. From Equation (3.5), the effective width can be derived as in Equation (5.5) [37], where it is assumed that 1) both of the skin and the stiffener are made of the same material, 2) the sheet has a continuous connection with the stiffener, and 3) the sheet with an effective width takes a uniform stress, which has the same total strength as the sheet under actual non-uniform stress distribution.

$$w = t \sqrt{\frac{k_c \pi^2 E}{12(1 - \nu^2) F_{ST}}} \quad (5.5)$$

In the stiffened panel structure used in the real aerospace structure, the material of sheet is generally different from that of stiffener. Hence, it is required that Equation (5.5) for the same material expands to the general case that the sheet and the stiffener have different material properties. Then Equation (5.5) for the effective width can be modified as Equation (5.6). [37]

$$w = t \frac{F_{SH}}{F_{ST}} \sqrt{\frac{\pi^2 k_c E_{SH}}{12(1-v^2)F_{ST}}} \quad (5.6)$$

where F_{SH} : Sheet stress existing at the same strain as existing for the stiffener

F_{ST} : Stress in the stiffener

E_{SH} : Young's modulus of elasticity in compression of a sheet panel

v : Poisson's ratio of a sheet panel

t : Sheet thickness

Applying the stress-strain relation, F_{SH} and F_{ST} can be expressed as Equations (5.7) and (5.8). By substituting Equations (5.7) and (5.8) into Equation (5.6) and re-arranging, we obtain Equation (5.9).

$$F_{ST} = \sigma_n = E_{ST} \varepsilon \quad (5.7)$$

$$F_{SH} = \frac{E_{SH}}{1-v^2} \varepsilon = \frac{E_{SH} \sigma_n}{(1-v^2)E_{ST}} \quad (5.8)$$

$$w = \frac{t E_{SH}}{(1-v^2)E_{ST}} \sqrt{\frac{\pi^2 k_c E_{SH}}{12(1-v^2)\sigma_n}} \approx \gamma t \quad (5.9)$$

The effective width is originally the function of the sheet thickness and the normal stress of stringer. But, in order to make the following optimization process for structural sizing more efficient, we assume that the

internal loads in panel change slowly enough during optimization. It is notable that the effective width in Equation (5.9) can be expressed as the function of only sheet thickness because there is no stress update during the local level optimization with this assumption, that is, $\frac{\partial \sigma_n}{\partial t}$ would go to zero. In addition, this assumption also provides the rationale on decomposing a big problem into a set of small problems and solving them separately during multi-level optimization because the stress constraints become uncoupled with this assumption.

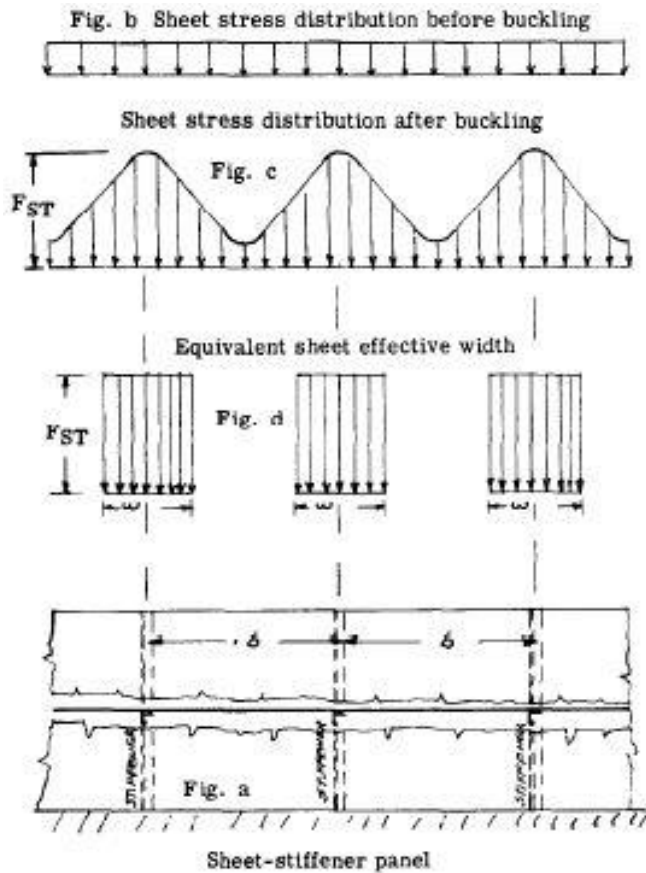


Figure 5.3 Stress Distribution before and after Buckling[37]

5.5 Computational Results

5.5.1 Load Generation

DIAMOND/AIRCRAFT is capable of importing the result of load analysis calculated from an external program using panel method or CFD for aerodynamic analysis. The aerodynamic loads calculated in the external program can be imported in the form of V-M-T curves (vertical shear force-moment-torsion), pressure or force distribution into the structural model using one of three methods.

① Using Linear algebra algorithm with V-M-T curves

It is assumed that the load imposed on a certain station is defined by a linear load equation. Using simple linear algebra algorithm, the load distribution is determined.

② Using V-M curves and Chord-wise distribution with C_p curve

This method is assumed that the load distribution along the chord-wise direction is subject to the C_p curve on a certain station. Through the scaling of C_p , V-M loads are distributed along the span-wise direction.

③ Using Discrete data transfer using spatial proximity search

When aerodynamic pressure is calculated using CFD, the data transfer technique is required for the state variable conversion such as pressure onto the nodes of FE mesh because of dissimilar meshes between CFD and CSM (Computational Structural Mechanics). [62]

As shown in Figure 5.4, the aerodynamic load is transferred on each node of FE mesh from three nearest nodes of CFD mesh, which are found through a spatial proximity search.

In order to carry out the minimum weight design of wing of 90-seat turboprop aircraft, the load condition is given as shown in Figure 5.5. The loads imposed on the wing consist of vertical shear force, moment, and torsion, which were generated by the external load analysis program. These V-M-T loads are distributed at 30 stations along the wing span, and then the imported load data is applied on FE meshes for the wing by the method. The C_p distribution at each station along the wing span is calculated through 2-dimensional CFD analysis. Using V-M curves along the wing span and C_p distribution along the chord length, the load distribution on the wing is determined. The engine weight is also reflected using concentrated mass element and connected to the hard points of wing using rigid link elements. The boundary conditions are fixed at the interface locations between the wing and the fuselage.

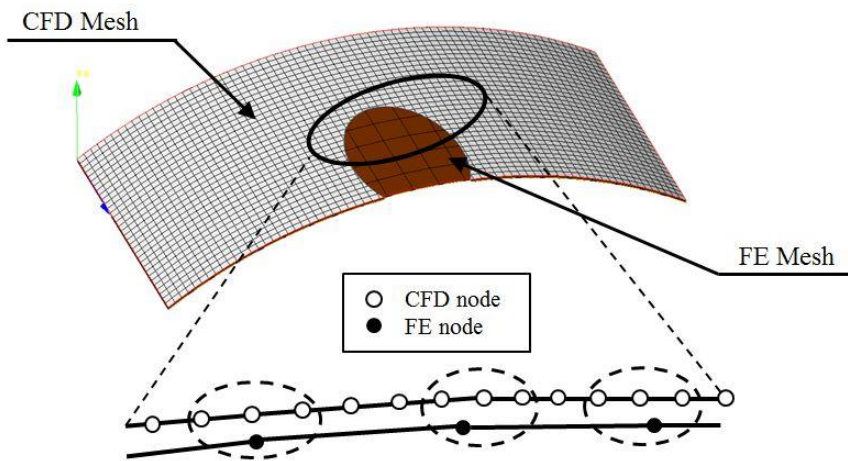


Figure 5.4 Data Transfer Technique between Dissimilar Meshes

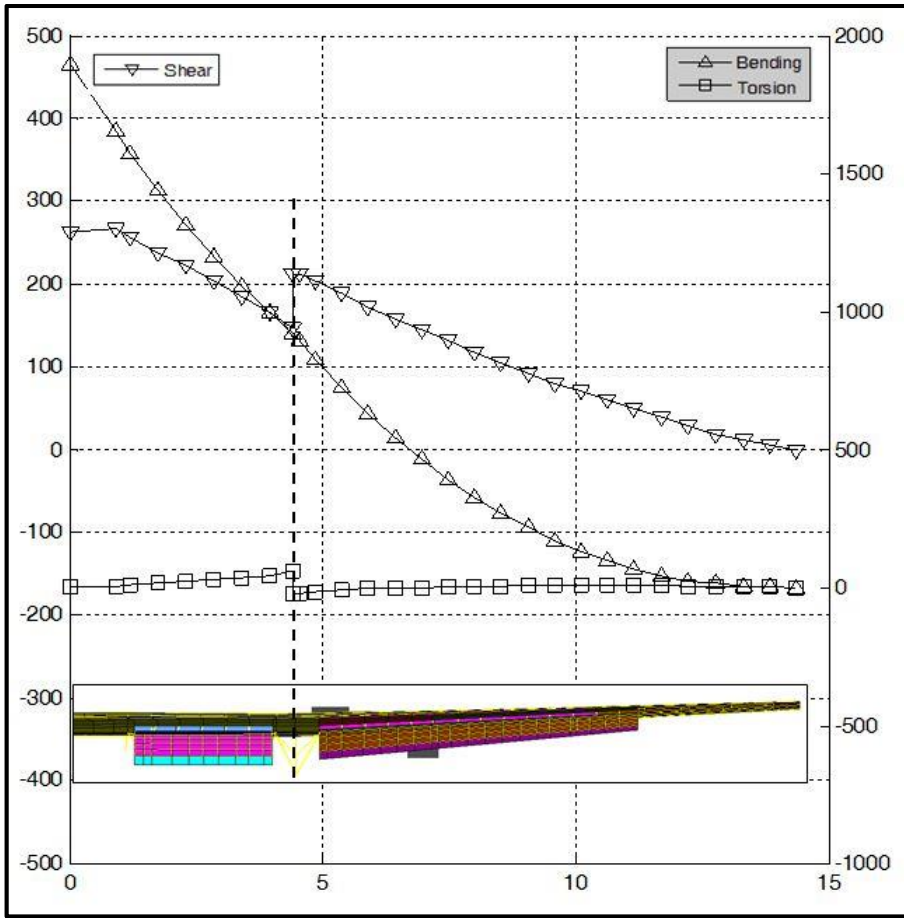


Figure 5.5 V-M-T Curves for Applied Load Condition

5.5.2 Minimum Weight Design

With the load conditions as shown in Figure 5.5, the minimum weight design is carried out for the wing of 90-seat turboprop aircraft. The optimization problem to be solved is represented in Chapter 5.3. Initially, FE model of the wing has seven stringers and thirty two ribs. All the structural members including skin, stringers, ribs, spars, and the like has the same initial thickness, 0.2 in. The design variables considered are skin thickness, the dimension of stringer, rib thickness, and spar thickness.

As shown in Figure 5.6, the minimum weight of wing is converged to 6,164 pounds when the effective width is taken into account. The effective width and the stress are updated in the global level during the optimization, while the effective width is constant in the local level optimization. After the stress is updated in the global level, it is found that the weight decreases dramatically compared with that in the previous step as shown in Figure 5.6. Because the stress used in the local optimization is what was calculated in the previous step of the global level, the stress used in the present step may be underestimated compared with the actual stress and then the weight might decrease excessively. But none of those points in the valley as shown in Figure 5.6 is the optimal design point that satisfies all the constraint functions given in the Chapter 5.3. That is, there is at least one violation for the constraint functions. So the weight increases to satisfy all the constraint conditions in the next step whenever the stress is updated again. The same pattern like this is already presented in Chapter 4.4.2. This kind of process is repeatedly performed until the optimal point is finally found.

Figures 5.7 and 5.8 show the distribution of upper and lower skin thickness for the wing, respectively. As the location of skin goes from wing root to wing tip, the thickness of upper skin generally becomes thinner. But, at three zones where the load is introduced, the skin thickness is thicker than in the neighborhood. The zone A is where the load is transferred from the inner flap as well as near the wing root. The engine nacelle is located in the zone B and connected to the primary structure of wing there. In two bays of the zone C, where the aerodynamic load in flight is transferred through the outer flap and the aileron, the skin thickness is relatively thicker than in the neighborhood. Unlike the upper skin where the compressive load is dominant, material strength is the main cause of failure in the lower skin because the tensile load is dominant. The distribution of thickness in the lower skin seems to be irregular compared with the upper skin where the thickness decreases toward the wing tip, but the thicker areas are found near the wing root and the load path connected to the control surfaces.

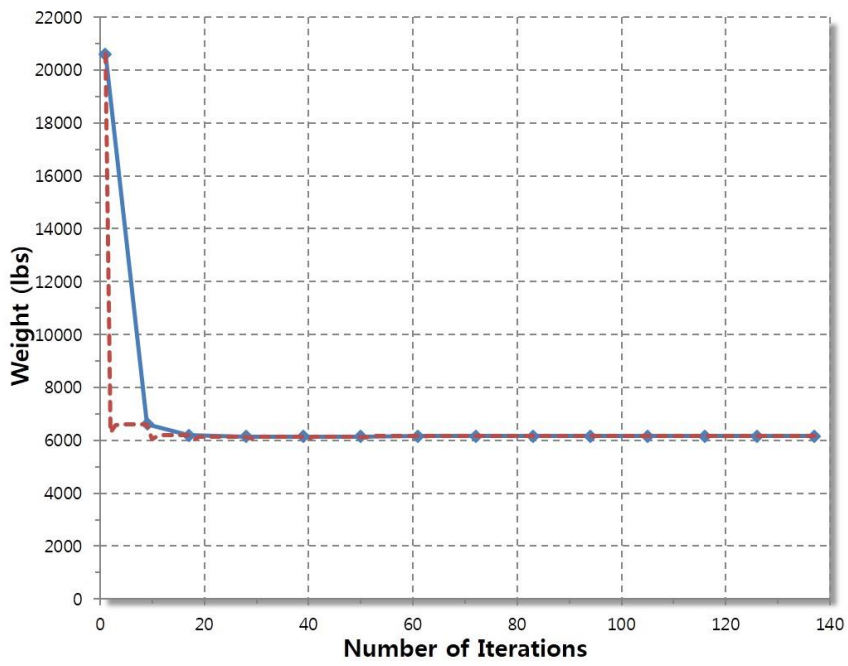


Figure 5.6 Convergence History of Wing Weight

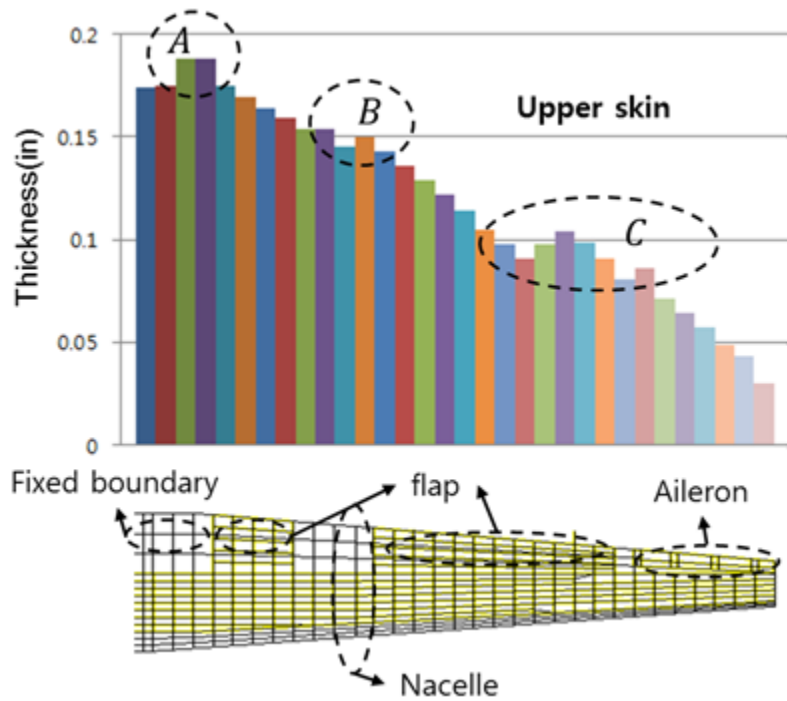


Figure 5.7 Distribution of Upper Skin Thickness

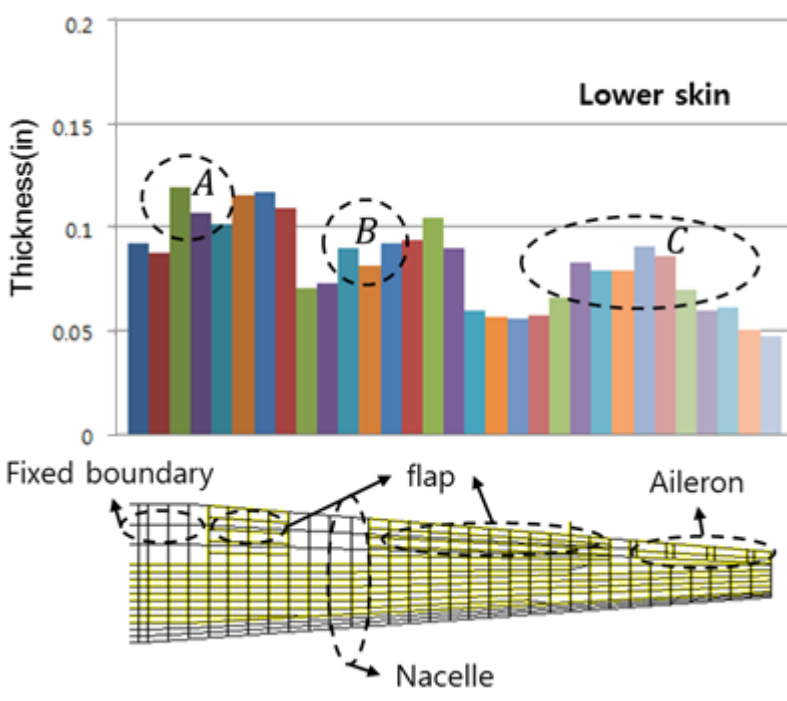


Figure 5.8 Distribution of Lower Skin Thickness

5.5.3 Parametric Study

The parametric study is performed with respect to the number of stringers and ribs, and it is investigated how the weight changes according to the quantity of two structural members. For the parametric study, the number of stringers ranges from six to thirteen, and the number of ribs from twenty six to thirty four.

First, the parametric study for the stringer is investigated. Figure 5.9 shows the weight change for the number of stringers. Rectangular symbols represent the case not considering the effective width, while diamond symbols represent the case considering the effective width. As results, it is confirmed that the optimum quantity of stringers is seven. The minimum weight of wing is 6,164 pounds considering the effective width. As expected, the lighter weight is obtainable when the effective width is considered. The difference of weight for effective width is 427 pounds ($6,591-6,164=427$). In the case of considering the effective width, the wing weight varies 6,164 to 6,496 pounds. Figure 5.10 shows the wing weight breakdown for the number of stringers. In the optimal design point with seven stringers, the skin weight is lighter than that with eight stringers by 65.1 pounds. The rib weight is also reduced by over 100 pounds. As results, total wing weight decreases although the stringer weight increases by nearly 100 pounds. As the number of stringers increases from eight, it is found that total wing weight would increase although the skin weight decreases by 76.3 pounds.

When the parametric study for the rib is carried out, the number of stringers is fixed at seven, the optimal quantity of stringers as shown in Figure

5.11. The rib weight is relatively small compared with the skin and the stringer weight. Among five cases, the minimum of skin weight and total wing weight occur at the wing structure with thirty two ribs as shown in Figure 5.12. In summary, similarly to the parametric study for the stringer, among the weights considering the effective weight is the optimal design point, which includes thirty two ribs.

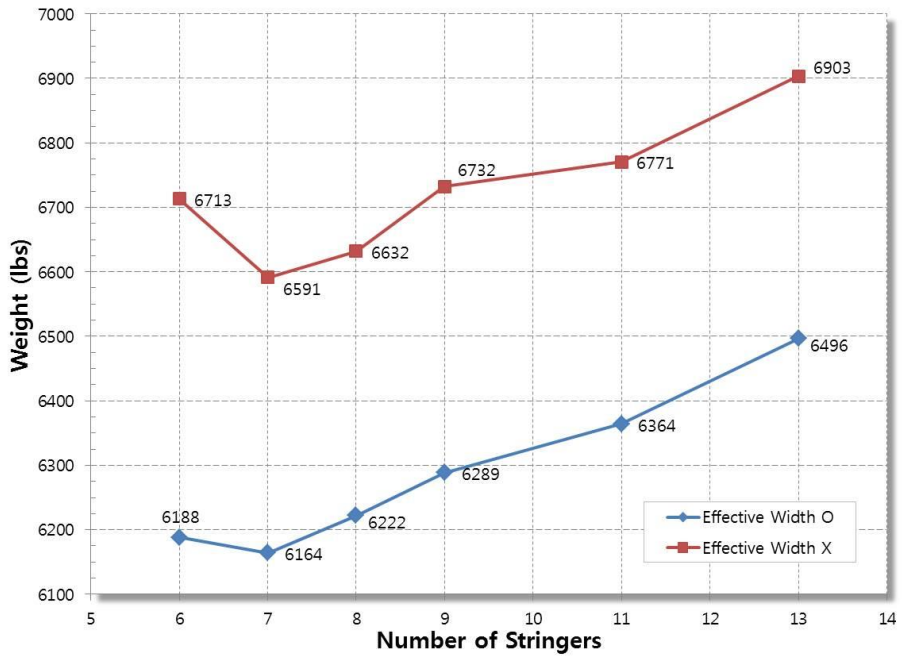


Figure 5.9 Wing Weight vs. the Number of Stringers

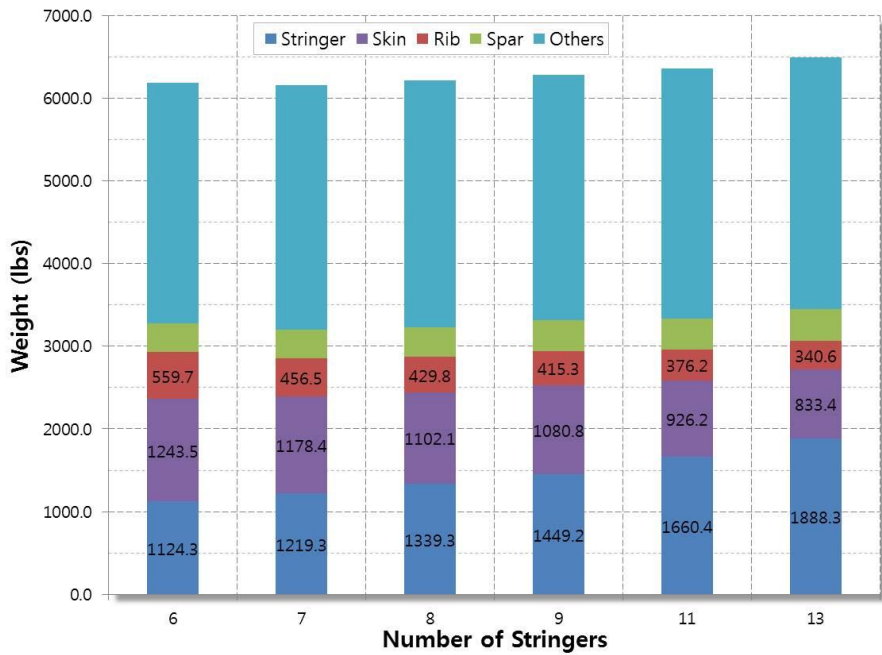


Figure 5.10 Wing Weight Breakdown for the Number of Stringers

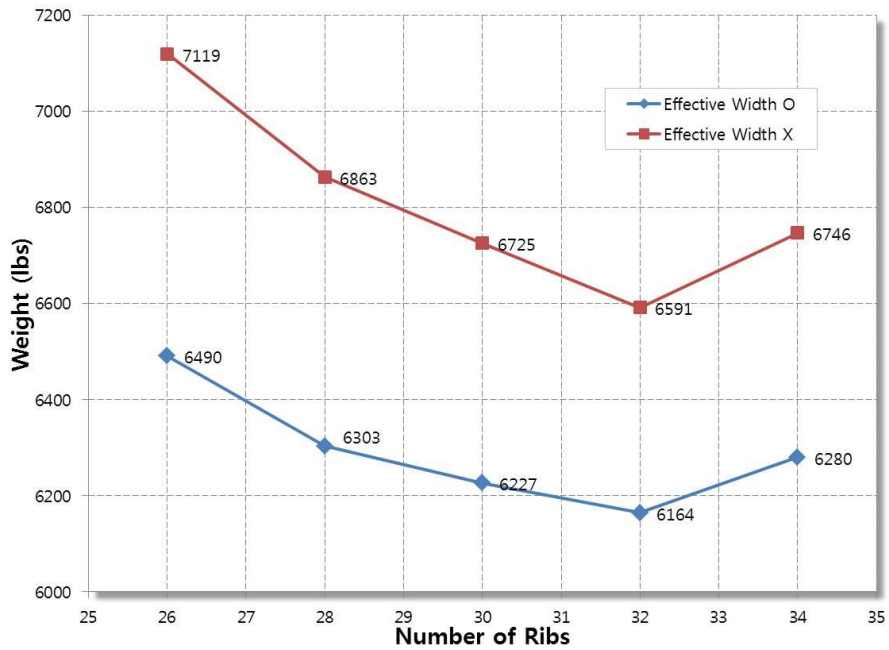


Figure 5.11 Wing Weight vs. the Number of Ribs

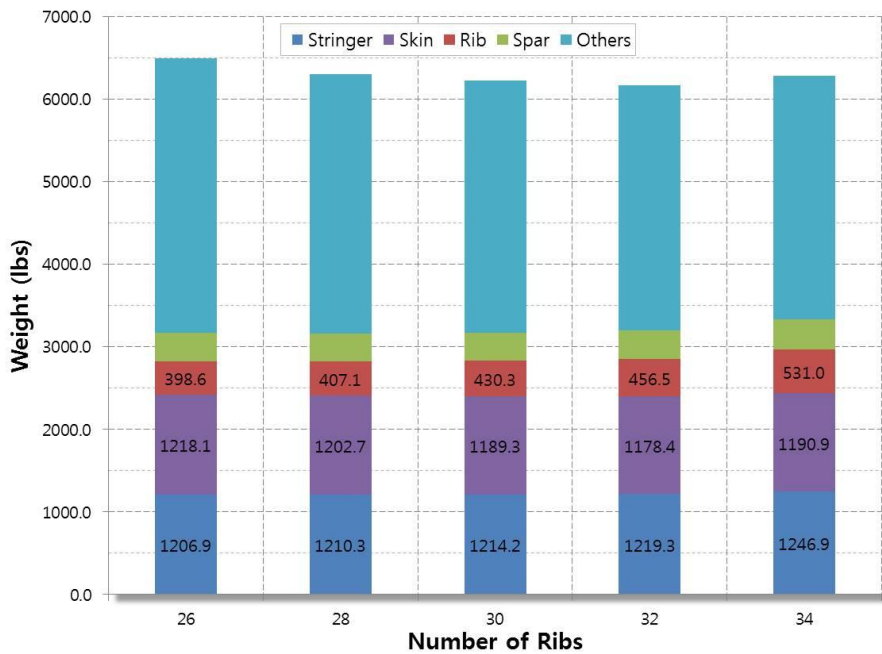


Figure 5.12 Wing Weight Breakdown for the Number of Ribs

5.5.4 Comparison with Empirical Methods

When the optimization for structural sizing is completed, the weight estimation is available by multiplying the volume and the density from FE model. Besides the result from a physics-based method, DIAMOND/AIRCRAFT can also provide weight estimations using conventional empirical methods proposed by Raymer [27] , Torenbeek [33], and Corke [63]. Figure 5.13 shows GUI of weight estimation module called COCOA using empirical methods.

The weight estimations of wing were calculated using four empirical methods and a physics-based method in DIAMOND/AIRCRAFT. Table 5.3 summarizes the comparison of weight estimations of wing among applied methods. As a result, two empirical methods generally tend to underestimate the weight of wing, except the method by Torenbeek. The weight estimations using empirical methods range from -20.45 to 15.32% difference, at least more than 15% difference, as compared with the reference weight, while the physics-based approach using DIAMOND/AIRCRAFT produces less than 5% difference. As results, it is confirmed that the weight estimation from the physics-based approach is closer to the reference weight than any other estimation by empirical methods.

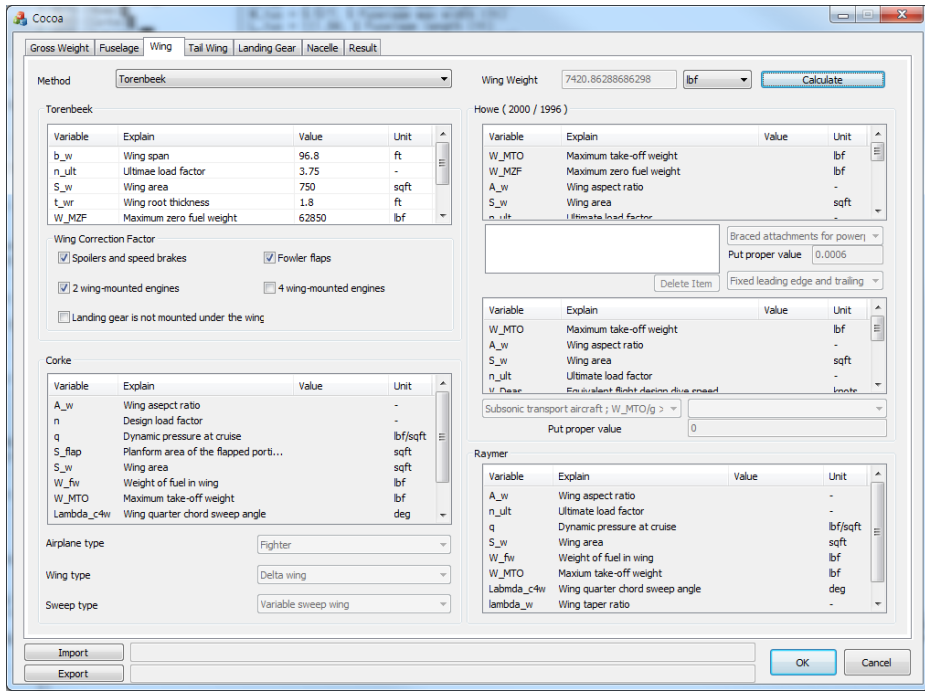


Figure 5.13 GUI of COCOA for Empirical Weight Estimation

Table 5.3 Comparison of Weight Estimations for Wing

Estimation Method		Weight (lbs)	Difference (%)
Empirical Method	Torenbeek	7,421	15.32
	Raymer	5,119	-20.45
	Corke	5,275	-18.03
Physics-based Method		6,164	-4.21
Reference		6,435	-

Chapter 6 Conclusion

This dissertation proposes the newly developed design framework, DIAMOND/AIRCRAFT, which is applicable to the early design phase for aircraft. The design framework utilizes the parametric modeling technique in order to efficiently deal with the labor-intensive and iterative model updating according to design changes. DIAMOND/AIRCRAFT can construct FE model through automated mesh generation, and the design work can be improved and facilitated with respect to the productivity. It should be also highlighted that DIAMOND/AIRCRAFT can estimate the structural weight based on a physics-based approach using high-fidelity method, FEM. DIAMOND/AIRCRAFT can produce the structural model considering the secondary structure as well as the primary structure, while other similar design tools can deal with the primary structure only.

In order to efficiently implement the optimization for aircraft structure, multi-level optimization routine is developed using augmented Lagrangian Method (ALM). This approach is adequate to solving a large-scale problem such as complex aerospace structure efficiently. By help of ALM, the highly nonlinear local constraints such as crippling, buckling and material strength can be processed with numerical stability. The local design variables such as dimensions of stringer and thickness of skin and rib are optimized in consideration of various design criteria such as buckling, crippling, and material strength for beam and shell structures. Because the primary structure of aerospace vehicles involves the stiffened panel structure,

the skin structure participates in bearing compressive load partly with the stringer. Hence, effective width method is utilized in the structural design to achieve the goal of weight saving. Being originally a function of both stress and skin thickness, the effective width is simplified as a function of only skin thickness by the introduction of appropriate physical assumption to improve the computational efficiency.

As a case study, the structural design of wing for 90-seat turboprop aircraft is carried out. With the parametric modeling function of DIAMOND/AIRCRAFT, elapsed time for generating FE model can be considerably reduced up to only a few minutes, while it takes several days to generate FE model of aircraft with a conventional FE modeler. Based on the more realistic model, the weight estimation from the physics-based method makes a good agreement with the reference weight more accurately. It is expected that the value of physics-based design framework will stand out when an unconventional advanced aircraft with no empirical weight data is developed rather than a conventional 'tube-and-wing' aircraft.

Bibliography

- [1] Sohlenius, G., “Concurrent Engineering,” *CIRP Annals-Manufacturing Technology*, vol. 95, 1992, pp. 645–655.
- [2] Sadraey, M. H., *Aircraft Design: A Systems Engineering Approach*, West Sussex, UK: John Wiley and Sons, Ltd., 2013.
- [3] Rosenblatt, A., and Watson, G., “Concurrent engineering,” *IEEE Spectrum*, 1997, pp. 22–37.
- [4] Gloudemans, J., Davis, P., and Gelhausen, P., “A Rapid Geometry Modeler for Conceptual Aircraft,” *Proceedings of the 34th Aerospace Sciences Meeting*, 1996, pp. 1–9.
- [5] Rodriguez, D. L., and Sturdza, P., “A Rapid Geometry Engine for Preliminary Aircraft Design,” *44th AIAA Aerospace Sciences Meeting and Exhibit*, Reno, NV: 2006, pp. 1–12.
- [6] Hahn, A. S., “Vehicle sketch pad: a parametric geometry modeler for conceptual aircraft design,” *48th AIAA Aerospace Sciences Meeting Including the New Horizons Forum and Aerospace Exposition*, Orlando, Florida: 2010, pp. 1–12.
- [7] Mawhinney, P., Price, M., Curran, R., and Benard, E., “Geometry Approach to Analysis Integration for Aircraft Conceptual Aircraft Conceptual Design,” *AIAA 5th Aviation, Technology, Integration, and Operations Conference (ATIO)*, Arlington, Virginia: 2005, pp. 1–9.
- [8] Amadori, K., Jouannet, C., and Krus, P., “A Framework for Aerodynamic and Structural Optimization in Conceptual Design,” *25th AIAA Applied Aerodynamics Conference*, Miami, FL: 2007, pp. 1–10.
- [9] Laughlin, T. W., Corman, J. a, and Mavris, D. N., “A Parametric and Physics-Based Approach to Body Aircraft,” *51st AIAA Aerospace Sciences Meeting including the New Horizons Forum and Aerospace Exposition*, 2013, pp. 1–20.
- [10] Sarakinos, S. S., Valakos, I. M., and Nikolos, I. K., “A software tool for generic parameterized aircraft design,” *Advances in Engineering Software*, vol. 38, 2007, pp. 39–49.

- [11] Azamatov, A., Lee, J.-W., and Byun, Y.-H., “Comprehensive aircraft configuration design tool for Integrated Product and Process Development,” *Advances in Engineering Software*, vol. 42, Jan. 2011, pp. 35–49.
- [12] Suwaratana, D. L., and Rodriguez, D. L., “A More Efficient Conceptual Design Process Using the RAGE Geometry Modeler,” *49th AIAA Aerospace Sciences Meeting including the New Horizons Forum and Aerospace Exposition*, Orlando, Florida: 2011, pp. 1–10.
- [13] Chen, B., Luo, M., Shen, Z., Wu, Z., Man, Y., and Fang, L., “Wing weight estimation considering constraints of structural strength and stiffness in aircraft conceptual design,” *International Journal of Aeronautical and Space Sciences*, vol. 15, 2014, pp. 383–395.
- [14] Silva, J., and Chang, K., “Design Parameterization for Concurrent Design and Manufacturing of Mechanical Systems,” *Concurrent Engineering*, vol. 10, 2011, pp. 3–14.
- [15] Mukhopadhyay, V., “A Conceptual Aerospace Vehicle Structural System Modeling, Analysis and Design Process,” *48th AIAA/ASME/ASCE/AHS/ASC Structures, Structural Dynamics, and Materials Conference*, Honolulu, Hawaii: 2007, pp. 1–14.
- [16] Martin, J. N., “Processes for engineering a system: an overview of the ANSI/EIA 632 standard and its heritage,” *Systems engineering*, vol. 3, 2000, pp. 1–26.
- [17] Rizzi, A., “Modeling and simulating aircraft stability and control—The SimSAC project,” *Progress in Aerospace Sciences*, vol. 47, Nov. 2011, pp. 573–588.
- [18] Bindolino, G., Ghiringhelli, G., Ricci, S., and Terraneo, M., “Multilevel Structural Optimization for Preliminary Wing-Box Weight Estimation,” *Journal of Aircraft*, vol. 47, Mar. 2010, pp. 475–489.
- [19] Cavagna, L., Ricci, S., and Travaglini, L., “NeoCASS: An integrated tool for structural sizing, aeroelastic analysis and MDO at conceptual design level,” *Progress in Aerospace Sciences*, vol. 47, 2011, pp. 621–635.
- [20] Dorbath, F., Nagel, B., and Gollnick, V., “Extended physics-based wing mass estimation in early design stages applying automated model generation,” *Proceedings of the Institution of Mechanical Engineers, Part G: Journal of Aerospace Engineering*, vol. 228, 2013, pp. 1010–1019.

- [21] Roskam, J., *Airplane Design*, Kansas: DAR Corporation, 2003.
- [22] Torenbeek, E., *Advanced Aircraft Design*, West Sussex, UK: John Wiley and Sons, Ltd., 2013.
- [23] Ardema, M. D., Chambers, M. C., Patron, A. P., Hahn, A. S., Miura, H., and Moore, M. D., *Analytical Fuselage and Wing Weight Estimation of Transport Aircraft*, 1996.
- [24] Howe, D., *Aircraft Conceptual Design Synthesis*, Professional Engineering Publishing, 2000.
- [25] Shanley, F. R., *Weight-Strength Analysis of Aircraft Structures*, New York: Dover Publication Inc., 1950.
- [26] Elham, A., La Rocca, G., and Van Tooren, M. J. L., “Development and implementation of an advanced, design-sensitive method for wing weight estimation,” *Aerospace Science and Technology*, vol. 29, 2013, pp. 100–113.
- [27] Raymer, D. P., *Aircraft Design: A Conceptual Approach*, AIAA Inc., 2006.
- [28] “Concurrent Engineering” Available: https://en.wikipedia.org/wiki/Concurrent_engineering.
- [29] Sobieszczanski-Sobieski, J., and Haftka, R., “Multidisciplinary aerospace design optimization: survey of recent developments,” *Structural optimization*, vol. 14, 1997, pp. 1–23.
- [30] La Rocca, G., and Van Tooren, M. J. L., “Enabling Distributed Multi-disciplinary Design of Complex Products: A knowledge Based Engineering Approach,” *Journal of Design Research*, vol. 5, 2007, pp. 333–352.
- [31] Kim, S.J., Moon, J., K., and Kim, M. K., “Capabilities and Performance of General Purpose Parallel Finite Element Program, DIAMOND/IPSAP,” *Proceeding of Tri-University Workshop on Aero-Structural Mechanics & Aerospace Engineering (NASPC/TUWMA2008)*, Beijing, China: 2008.
- [32] Kim, J. H., Lee, C. S., and Kim, S. J., “High-Performance Domainwise Parallel Direct Solver for Large-Scale Structural Analysis,” *AIAA Journal*, vol. 43, 2005, pp. 662–670.

- [33] Torenbeek, E., *Synthesis of Subsonic Airplane Design*, Dordrecht, The Netherlands: Kluwer Academic Publishers, 1982.
- [34] LANSING, W., DWYER, W., EMERTON, R., and RANALLI, E., “Application of Fully Stressed Design Procedures to Wing and Empennage Structures,” *Journal of Aircraft*, vol. 8, Sep. 1971, pp. 683–688.
- [35] Patnaik, S., and Hopkins, D., “Optimality of a fully stressed design,” *Computer Methods in Applied Mechanics and Engineering*, vol. 165, 1998, pp. 215–221.
- [36] Niu, M. C.-Y., *Airframe Stress Analysis and Sizing*, Hong Kong: Conmilit Press Ltd., 1997.
- [37] Bruhn, E. F., *Analysis and Design of Flight Vehicle Structures*, Tri-State Offset Company, 1973.
- [38] sourceforge.net, “Engauge Digitizer 5.1,” 2012.
- [39] Lasdon, L. S., *Optimization Theory for Large Systems*, Mineola, NY: Dover Publications Inc., 2002.
- [40] Boyd, S., and Vandenberghe, L., *Convex Optimization*, New York: Cambridge University Press, 2004.
- [41] Sobieszczanski-sobieski, J., “Optimization by Decomposition: A Step from Hierarchic to Non-Hierarchic Systems,” *2nd NASA/Air force Symp. on Recent Advances in Multidisciplinary Analysis and Optimization*, Hampton, VA: .
- [42] Shankar, J., Haftka, R. T., and Watson, L. T., “Computational study of a nonhierarchical decomposition algorithm,” *Computational Optimization and Applications*, vol. 2, 1993, pp. 273–293.
- [43] Kroo, I., Altus, S., Braun, R., Gage, P., and Sobieski, I., “Multidisciplinary Optimization Methods for Aircraft Preliminary Design,” *Fifth AIAA/USAF/NASA/ISSMO Symposium on Multidisciplinary Analysis and Optimization*, 1994, pp. 697–707.
- [44] Braun, R. D., and Kroo, I. M., “Development and Application of the Collaborative Optimization Architecture in a Multidisciplinary Design Environment,” *Multidisciplinary Design Optimization: State of the Art*, 1995, pp. 98–116.

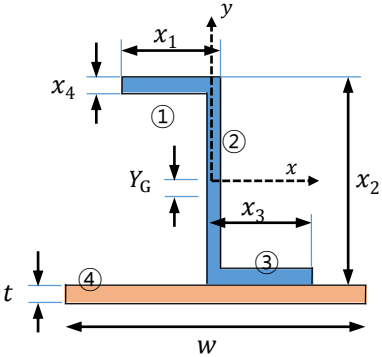
- [45] Braun, R., Moore, A., and Kroo, I., "Use of the collaborative optimization architecture for launch vehicle design," *6th Symposium on Multidisciplinary Analysis and Optimization*, 1996, pp. 306–318.
- [46] Sobieski, I., and Kroo, I., "Aircraft design using collaborative optimization," *AIAA 34th Aerospace Sciences Meeting and Exhibit*, 1996, pp. 1–11.
- [47] Schmit, L. A., and Ramanathan, R. K., "Multilevel Approach to Minimum Weight Design Including Buckling Constraints," *AIAA Journal*, vol. 16, Feb. 1978, pp. 97–104.
- [48] Schmit, L. A., and Mehrinfar, M., "Multilevel Optimum Design of Structures with Fiber-Composite Stiffened-Panel Components," *AIAA Journal*, vol. 20, 1982, pp. 138–147.
- [49] Sobieszczanski, J., and Loendorf, D., "A mixed optimization method for automated design of fuselage structures.," *Journal of Aircraft*, vol. 9, 1972, pp. 805–811.
- [50] Sobieszczanski-Sobieski, J., James, B., and Dovi, A., "Structural optimization by multilevel decomposition," *AIAA journal*, vol. 23, 1985, pp. 1775–1782.
- [51] Sobieszczanski-Sobieski, J., and Kodiyalam, S., "BLISS/S: a new method for two-level structural optimization," *Structural and Multidisciplinary Optimization*, vol. 21, Feb. 2000, pp. 1–13.
- [52] Williams, F. W., Kennedy, D., Anderson, M. S., and Butler, R., "VICONOPT - Program for exact vibration and buckling analysis or design of prismatic plate assemblies," *AIAA Journal*, vol. 29, 1991, pp. 1927–1928.
- [53] Wittrick, W. H., and Williams, F. W., "Buckling and vibration of anisotropic or isotropic plate assemblies under combined loadings," *International Journal of Mechanical Sciences*, vol. 16, 1974, pp. 209–239.
- [54] Anderson, M. S., and Stroud, W. J., "A general panel sizing computer code and its application to composite structural panels," *AIAA Journal*, vol. 17, 1978, pp. 892–897.
- [55] Bushnell, D., "PANDA-INTERACTIVE PROGRAM FOR MINIMUM WEIGHT DESIGN OF STIFFENED CYLINDRICAL PANELS AND SHELLS," *Computers & Structures*, vol. 16, 1983, pp. 1–4.

- [56] Bushnell, D., “FOR MINIMUM WEIGHT DESIGN,” 1987.
- [57] Bushnell, D., and Bushnell, W. D., “Minimum-weight design of a stiffened panel via PANDA2 and evaluation of the optimized panel via STAGS,” *Computers & Structures*, vol. 50, 1994, pp. 569–602.
- [58] Carrera, E., Mannella, L., Augello, G., and Gualtieri, N., “A two-level optimization feature for the design of aerospace structures,” *Proceedings of the Institution of Mechanical Engineers, Part G: Journal of Aerospace Engineering*, vol. 217, 2003, pp. 189–206.
- [59] Bertsekas, D. P., *Constrained Optimization and Lagrange Multiplier Methods*, Belmont, MA: Athena Scientific, 1996.
- [60] Arora JS, Chahande AI, P. J., “Multiplier methods for engineering optimization,” *International Journal for Numerical Method in Engineering*, vol. 32, 1991, pp. 1485–1525.
- [61] Nocedal, J., and Wright, S. J., *Numerical Optimization*, New York, NY: Springer Science+Business Media, LLC, 2006.
- [62] Samareh, J. a, “Discrete Data Transfer Technique for Fluid–Structure Interaction,” *18th AIAA Computational Fluid Dynamics Conference*, Miami, FL: 2007, pp. 1–12.
- [63] Corke, T. C., *Design of Aircraft*, Prentice Hall, 2003.

Appendix A: Partial Derivatives of Normal Stress for Beam

Cross Section Shape	Z	I	L
Description			
Design Variables	x_1, x_2, x_3, x_4	x_1, x_2, x_3, x_4	x_1, x_2, x_3
Area (A)	$x_4(x_1 + x_2 + x_3 - 2x_4) + \gamma t^2$		$x_3(x_1 + x_2 - x_3) + \gamma t^2$
Partial Derivatives of Normal Stress	$\frac{\partial \sigma_n}{\partial x_i} = -\frac{x_4}{A} \sigma_n \quad (i = 1, 2, 3)$ $\frac{\partial \sigma_n}{\partial x_4} = \frac{2x_4 - x_1 - x_2 - x_3}{A} \sigma_n$		$\frac{\partial \sigma_n}{\partial x_i} = -\frac{x_3}{A} \sigma_n \quad (i = 1, 2)$ $\frac{\partial \sigma_n}{\partial x_3} = \frac{2x_3 - x_1 - x_2}{A} \sigma_n$

Appendix B: Moment of Inertia for Z-type Beam

<p>Description</p>		
<p>Center of Cross Section (Y_G)</p>		$-\frac{\gamma(x_2 t^2 + t^3)}{2A}$
<p>Area (A)</p>		$x_4(x_1 + x_2 + x_3 - 2x_4) + \gamma t^2$
<p>I_{xx}</p>	<p>①</p>	$\frac{1}{12} x_1 x_4^3 + x_1 x_4 \left(\frac{x_2}{2} - \frac{x_4}{2} + Y_G \right)^2$
	<p>②</p>	$\frac{1}{12} x_4 (x_2 - 2x_4)^3 + x_4 (x_2 - 2x_4) Y_G^2$
	<p>③</p>	$\frac{1}{12} x_3 x_4^3 + x_3 x_4 \left(\frac{x_2}{2} - \frac{x_4}{2} - Y_G \right)^2$
	<p>④</p>	$\frac{1}{12} \gamma t^4 + \gamma t^2 \left(\frac{t}{2} + \frac{x_2}{2} - Y_G \right)^2$
<p>I_{yy}</p>	<p>①</p>	$\frac{1}{12} x_4 x_1^3 + x_1 x_4 \left(\frac{x_1}{2} - \frac{x_4}{2} \right)^2$
	<p>②</p>	$\frac{1}{12} (x_2 - 2x_4) x_4^3$
	<p>③</p>	$\frac{1}{12} x_4 x_3^3 + x_3 x_4 \left(\frac{x_1}{2} - \frac{x_3}{2} \right)^2$
	<p>④</p>	$\frac{1}{12} t w^3$

초 록

본 논문에서는 항공기 구조물 설계에 적용하기 위한 다중레벨 최적화 기법에 대한 연구를 수행하였다. 우선 항공기 설계 초기단계에서 사용할 수 있는 효율적인 구조설계 프레임워크를 개발하였다. 항공기 설계 초기과정에서는 다양한 후보형상에 대한 비교검토를 수행해야 하는 설계의 특성상 불가피한 설계 모델의 반복적인 생성 및 변경을 자동화하여 설계 효율을 증진시킬 수 있는 설계 도구의 필요성이 대두되었다. 따라서 항공기 설계에 특화된 설계인자를 매개변수화하여 설계자가 사용하기에 간편하면서도 신속하게 항공기 내부 구조배치까지 고려한 구조설계 모델을 생성할 수 있는 설계 프레임워크를 개발하였다. 본 연구에서 개발한 설계 프레임워크는 하중을 주로 담당하는 1차 구조물뿐만 아니라 2차 구조물까지 포함하여 실제 구조물에 가까운 구조모델을 생성하는 것이 가능하다는 장점도 가진다.

항공기 구조물처럼 복잡하고 거대한 다자유도 구조해석 문제를 효율적으로 풀기 위해서는 하나의 큰 문제를 여러 개의 작은 문제로 분할하여 계산하는 것이 유리하다고 알려져 있다. 본 논문에서는 다중레벨 최적화 기법을 적용하여 항공기 날개 구조물을 베이(Bay) 단위로 분할하여 날개 전체에 대한 구조 최적화를 수행하였다. 이 과정에서 Augmented Lagrangian Method를 사용하여 설계기준으로 적용된 다양한 구속조건들을 목적함수에 포함시킴으로써 구속조건 문제를 무구속조건 문제로 변환하여 최적화 문제를 효율적으로 계산할 수 있었다. 스킨, 스트링거, 스파, 리브의 두께를 설계변수로 설정하고, 좌굴, 크리플링, 국부적 후좌굴 등을 설계기준으로 고려하였다. 최적화 과정 중에 계산되는 응력과 유효폭은 전역 수준에서만 최신택되며, 국부 수준에서 수행되는 최적화 계산에서는 고정된 값으로 계산이 수행된다. 이 때, 적절한 물리적 가정을 도입하여 스킨의 유효폭을 스킨 두께만의 함수로

한정시킴으로써 최적화 과정 중에 발생하는 계산량을 줄이고 풀이과정을 단순화하는데 기여하였다.

본 논문에서 개발한 매개변수 모델링이 가능한 물리기반의 설계 프레임워크를 직접 사용하여 90인승 중형항공기의 날개에 대한 구조 사이징을 수행하였다. 통상 수 일이 걸리는 유한요소모델 생성시간을 매개변수 모델링 기법을 통해 수 분 수준으로 단축할 수 있었고, 다중레벨 최적화 방법을 사용하여 복잡한 구조물의 해석을 효율적으로 수행하는 동시에 물리기반 방법을 통한 중량예측이 기존의 통계적인 방법보다 정확한 중량예측이 가능함을 확인하였다. 이로써 개발된 설계 프레임워크가 실제 항공기 제작현장에서 적용될 수 있는 가능성을 제시하였다. 또한 이러한 물리기반 접근방법은 통계적인 자료가 존재하지 않는 신개념 항공기를 개발할 경우에 더욱 유용할 것으로 기대한다.

주요어 : 다중레벨 최적화, 매개변수 모델링, 물리기반 설계,
설계 프레임워크, 구조 사이징, 중량예측

학 번 : 2010-30201